Genesis of twin tropical cyclones as revealed by a global mesoscale model: The role of mixed Rossby gravity waves

Bo-Wen Shen,[1,2] Wei-Kuo Tao,[2] Yuh-Lang Lin,[3] and Arlene Laing[4]

Received 12 January 2012; revised 26 April 2012; accepted 29 May 2012; published 12 July 2012.

[1] In this study, it is proposed that twin tropical cyclones (TCs), Kesiny and 01A, in May 2002 formed in association with the scale interactions of three gyres that appeared as a convectively coupled mixed Rossby gravity (ccMRG) wave during an active phase of the Madden-Julian Oscillation (MJO). This is shown by analyzing observational data, including NCEP reanalysis data and METEOSAT 7 IR satellite imagery, and performing numerical simulations using a global mesoscale model. A 10-day control run is initialized at 0000 UTC 1 May 2002 with grid-scale condensation but no sub-grid cumulus parameterizations. The ccMRG wave was identified as encompassing two developing and one non-developing gyres, the first two of which intensified and evolved into the twin TCs. The control run is able to reproduce the evolution of the ccMRG wave and thus the formation of the twin TCs about two and five days in advance as well as their subsequent intensity evolution and movement within an 8–10 day period. Five additional 10-day sensitivity experiments with different model configurations are conducted to help understand the interaction of the three gyres, leading to the formation of the TCs. These experiments suggest the improved lead time in the control run may be attributed to the realistic simulation of the ccMRG wave with the following processes: (1) wave deepening (intensification) associated with a reduction in wavelength and/or the intensification of individual gyres, (2) poleward movement of gyres that may be associated with boundary layer processes, (3) realistic simulation of moist processes at regional scales in association with each of the gyres, and (4) the vertical phasing of low- and mid-level cyclonic circulations associated with a specific gyre.

Citation: Shen, B.-W., W.-K. Tao, Y.-L. Lin, and A. Laing (2012), Genesis of twin tropical cyclones as revealed by a global mesoscale model: The role of mixed Rossby gravity waves, *J. Geophys. Res.*, *117*, D13114, doi:10.1029/2012JD017450.

1. Introduction

[2] Accurately forecasting tropical cyclone (TC) genesis, frequency, intensity and movement is crucial in preventing loss of life and property as well as studying TC inter-annual variability and the impact of climate change on long-term TC variations. Over the past several decades, TC track forecasts have steadily improved, but intensity and genesis forecasts have lagged behind. One of the major challenges in TC genesis prediction is the accurate simulation of complex interactions across a wide range of scales, from the large-scale environment (deterministic), to mesoscale flows, down to convective-scale motions (stochastic).

[3] Using global models for TC prediction is a natural choice for achieving the goal of studying TC inter-annual variability, because these models can simulate multiscale flows globally (e.g., large-scale tropical waves) and thus reduce the errors that may be associated with the use of regional numerical models. For example, these errors may come from the use of time-varying lateral boundary conditions from global analyses and the inherited limitation of the one-way interactions between a TC and its environmental flows that are provided by the global analyses. However, the goal of improving short-term forecasts of TC intensity and formation on a regional scale is still very challenging because such a global model would require sufficient resolution to accurately represent fine-scale physical and dynamical processes as well as respond to warm sea surface temperatures [e.g., *Bengtsson et al.*, 2007a, 2007b] and thereby demands tremendous computing resources. Modern supercomputing technology has made it possible to employ ultra-high resolution GCMs [*Kerr*, 2006] and as a result obtain remarkable short-term forecasts of hurricane track and intensity [e.g., *Atlas et al.*, 2005; *Shen et al.*, 2006a, 2006b, 2006c].

[1]Earth System Science Interdisciplinary Center, University of Maryland, College Park, Maryland, USA.
[2]NASA Goddard Space Flight Center, Greenbelt, Maryland, USA.
[3]Department of Physics, North Carolina Agricultural and Technical State University, Greensboro, North Carolina, USA.
[4]UCAR/COMET, Boulder, Colorado, USA.

Corresponding author: B.-W. Shen, NASA Goddard Space Flight Center, Code 612, Greenbelt, MD 20771, USA. (bo-wen.shen-1@nasa.gov)

Motivated by the scientific challenge and encouraged by the preliminary success with a global mesoscale model [e.g., *Shen et al.*, 2010a] which was originally developed as a climate model, the objective now is to extend TC studies from TC short-term forecasts to TC climate simulations, beginning with examining the model's ability to simulate the multiscale processes associated with different kinds of tropical waves (such as MRG waves and African easterly waves, AEWs) and their scale interactions that lead to TC genesis.

[4] Hurricane models, along with guidance from observations, have been used to help construct TC theories since the 1960s. Two major intensification mechanisms [e.g., *Lin*, 2007] are CISK (conditional instability of the second kind) [*Charney and Eliassen*, 1964; *Ooyama*, 1964] and air-sea interaction (wind-induced surface heat exchange –WISHE) [*Emanuel*, 1986], both of which assume the existence of a pre-TC disturbance. These mechanisms focus on the so-called cooperative interactions between the primary (vortex-scale) circulation and the secondary circulation [*Ooyama*, 1969] and have been used to explain the physical processes of TC intensification during a TC's mature stage with some degree of satisfaction. However, their validity in depicting the intensity evolution for a weak TC and/or the initiation of the pre-TC disturbance is less known. From a modeling perspective, verification of these related processes relies on the accurate representation of moist processes and boundary/surface layer processes associated with cumulus parameterizations (CPs) [e.g., *Anthes*, 2003] and boundary/surface layer parameterizations [e.g., *Braun and Tao*, 2001], respectively. However, it has been documented that coarse-resolution model simulations are strongly influenced by these parameterizations, which often leads to large errors in track and intensity. In contrast to the concept of "cooperative interaction," a "vortex merger" mechanism that focuses on the upscaling feedback by small-scale vortices has been proposed to address the initial intensification during tropical cyclogenesis [e.g., *Hendricks et al.*, 2004; *Montgomery et al.*, 2006]; it states that the merging of small-scale vortices plays an essential role in TC formation. In particular, a moist vortex merger is more efficient than a dry one, producing stronger TC intensities at a relatively shorter time. Therefore, an ultra high-resolution (∼1–4 km) model with proper moist processes seems to be crucial for simulating TC formation, assuming vortex merger is an important component for genesis. In contrast to the fine-resolution runs, simulations of TC formation with a "coarse-resolution" (>∼10 km) regional model by *Nolan* [2007] suggested that axisymmetrization, instead of "vortex merger," may appear in association with vortex intensification. With a limited-area model at a comparable resolution, *Tory et al.* [2006a, 2006b] conducted short-term numerical experiments on a 0.15 degree (∼16 km) unstaggered grid and reported that TC formation can be predicted with a lead time of 24–36 h without the detailed simulation of small-scale convection.

[5] Despite the success of the aforementioned processes in explaining TC dynamics, further improvement in terms of realistically capturing the impacts associated with large-scale flows is still needed in order to understand long-term TC activity. For example, some of the aforementioned numerical models that were used for studying TC intensity evolution lack the ability to realistically simulate the two-way interaction between hurricanes and environmental flows (e.g., large-scale tropical waves). These include axisymmetric models with idealized initial flows and regional models with imposed initial environmental flow information and time-varying lateral boundary conditions from global analyses/reanalyses at an internal of 6h. In addition, the assumption of a pre-existing disturbance in hurricane theories has the advantage of putting the focus on the critical processes that happen just prior to TC genesis over a relatively short period of time, but only provide a short lead time for TC prediction. However, this kind of assumption does not address the dependence of these critical processes on the large-scale environmental processes that can initiate or impact the pre-existing disturbances. Thus, the assumption of a pre-existing disturbance needs to be removed or relaxed to consider the impact of (larger-scale) environmental flows on the formation of a pre-TC disturbance and its subsequent intensification. This can be important for extending the lead time of TC genesis prediction.

[6] In contrast to the focus on the small-scale processes that contribute to TC formation, *Holland and Webster* [2005] emphasized the importance of downscale energy and vorticity transfer associated with the accumulation of large-scale Rossby types of waves [*Webster and Chang*, 1988], which does not necessarily involve moist convection. They applied this idea to explain why a coarse-resolution (∼100 km) global model with the advantage of simulating large-scale flows could have skill with regard to TC genesis simulation. One implication of this is that an accurate representation of the evolution of the large-scale flow could "narrow" down the uncertainties in the area and period for TC formation [e.g., *Ooyama*, 1982]. Recent studies [e.g., *Frank and Roundy*, 2006; *Bessafi and Wheeler*, 2006; *Schreck et al.*, 2012] examined the role of different tropical waves in tropical cyclogenesis with observations. By analyzing NCEP-NCAR reanalyses (e.g., 850 and 200 hPa winds) and outgoing longwave radiation data, *Frank and Roundy* [2006] found a strong relationship between TC formation and enhanced activity in equatorial Rossby (ER) waves, mixed Rossby gravity (MRG) waves, TD-type disturbances (or easterly waves, EWs), or the Madden-Julian Oscillation (MJO) [*Madden and Julian*, 1994]. In addition, they pointed out the possibility of detecting the convective anomalies in waves associated with genesis up to 1 month in advance. Their results provide an observation basis for the predictive relationship between tropical waves and TC formation and thus suggest the possibility of extending the lead time of TC genesis prediction with numerical models. In comparison, by studying the frequency of TC genesis that is associated with tropical waves in different regions, *Schreck et al.* [2012] suggested that (1) TD-type disturbances were the most common TC precursor in the NH; (2) the number of TCs attributed to the TD-type disturbances and ER waves is roughly equivalent in the SH; (3) fewer TCs were attributed to MRG waves, Kelvin wave or the MJO. However, in an earlier study by *Bessafi and Wheeler* [2006], they concluded that statistical analysis of the TCs west of 100°E shows a significant modulation by the MJO and ER waves. Note that the ER, MRG and Kelvin wave modes were first studied by *Matsuno* [1966] with linearized shallow-water questions on a beta plane. In contrast, the TD-type disturbances and MJOs do not belong to the linear solutions to Matsuno's equations.

[7] The modulation of TC activity by an MJO has been documented and studied for more than a decade [e.g., *Liebmann et al.*, 1994; *Maloney and Hartmann*, 2000]. *Lander* [1990] showed that the eastward-moving MJO may have an impact on the nearly simultaneous formation of two TCs straddling the equator at low latitudes in the Indian Ocean and West Pacific Ocean. These TCs are called "twins," as they are "nearly" symmetric with respect to the equator. A restrictive definition on twin TCs proposed by *Lander* [1990] requires forming "nearly simultaneously" at the latitude of 5°N and 5°S and along the same longitude. In contrast, a twin TC was loosely defined by *Keen* [1982] as two TCs forming within 8–9 days of each other, within about 22° latitude and within a longitudinal difference of about 10°. The latter seems to be more applicable for daily weather forecasts. However, it will be shown that the degree (extent) of timing lag and longitudinal variations in the formation of the two consecutive TCs, one in the Northern Hemisphere (NH) and the other in the Southern Hemisphere (SH), may involve different intermediate physical processes, e.g., an ER wave versus MRG wave dynamics. While the well-documented solution of the linear MRG wave [e.g., *Matsuno*, 1966; *Wheeler et al.*, 2000; *Kiladis et al.*, 2009], will be briefly discussed in section 3.1, its impact on TC activity is briefly reviewed below.

[8] The linear MRG wave is a special wave mode that behaves like a Rossby wave for high zonal wave numbers and an inertio-gravity wave for low zonal wave numbers. While an ER wave is symmetric with respect to the equator, an MRG wave is antisymmetric with respect to the equator. Because of its asymmetric features, an MRG wave may lead to the successive formation of TCs at different longitudes with time lags in different hemispheres. Earlier studies suggested that lower-tropospheric MRG waves with 3–6-day periods were observed in different regions. Typical wavelengths of 7,000–10,000 km, a westward phase speed of 15–20 m/s and an eastward group speed of about 5 m/s were documented for the MRG waves in the central Pacific [e.g., *Dickinson and Molinari*, 2002, and references therein]. In comparison, shorter MRG waves with slower phase speeds were found in the western Pacific [e.g., *Liebmann and Hendon*, 1990, Figure 8]. For example, *Dickinson and Molinari* [2002] examined an MRG wave event with a wavelength of about 2300∼3000 km in the western Pacific. Note that *Molinari et al.* [2007] also documented a very short ER wave with a wavelength of 3600 km (wave number 11) and a phase speed of −1.9 m/s in the northwest Pacific. In addition to the horizontal 2D dynamics of a MRG wave, the vertical structure of the wave (i.e., phase tilting) may be influenced by moist processes and was examined by *Maruyama* [1967] and *Lindzen and Matsuno* [1968]. The impact of boundary layer processes, which may cause a TC to become cut off from a MRG wave, was examined by *Holton* [1975]. He pointed out that the phase relationship between the low geopotential height perturbation and convergence in a free MRG wave is distorted in a forced MRG wave with the inclusion of boundary layer friction.

[9] Based on the phase relationship of two fields, *Takayabu and Nitta* [1993] classified the 3–5 day-period disturbances into two types: MRG-wave type and TD type. The MRG-wave-type disturbance appears as a linear MRG wave with organized convection in the convergence region of the wave, i.e., the vertical motion is in phase with the meridional winds. In comparison, the TD-type disturbance has off-equatorial vortex train features with organized convection within a low pressure cyclonic vortex, which has the phase relationship similar to a forced MRG wave mode. Takayabu and Nitta then suggested that a MRG-type disturbance may turn into a TD-type disturbance as a result of boundary layer processes whereby its convergence zone becomes in phase with the low pressure center, leading to a vortex cutoff from the equator. Thus, TD-type disturbances may be viewed as off-equatorial westward propagating Rossby gyres [e.g., *Kiladis et al.*, 2009]. However, in practice, it is not easy to separate these two types (TD-type and MRG-type) of disturbances [e.g., *Straub and Kiladis*, 2003] because they occupy overlapping wave number-frequency space. Therefore, the term MRG-TD type disturbance, which often appear in the spectral or empirical orthogonal function analysis [e.g., *Frank and Roundy*, 2006, Figure 7; *Kiladis et al.*, 2009, Figure 12], is used to represent an MRG-type disturbance that may transition into a TD-type disturbance. Namely, a MRG-TD-type disturbance has a hybrid structure of the MRG-type and TD-type disturbances. In contrast to the boundary layer processes, *Chang and Webster* [1995] suggested that negative stretching deformation associated with an ER or a MRG wave can enable the latitudinal stretching and modify the wave number of the mode.

[10] The dynamics of "twin vortices" have been previously examined with shallow water equations or idealized simulations. For example, using idealized simulations, *Ferreira and Schubert* [1996] suggested the importance of westerly wind bursts (WWBs), which are associated with the MJO, in the formation of twin TCs, and emphasized the role of ER waves. The relationship between twin TC and an ER wave has been studied with observations [e.g., *Schreck and Molinari*, 2009, and references therein]. Recently, *Gall et al.* [2010] examined the role of ERs in TC genesis by conducting idealized simulations with the Weather Research and Forecasting (WRF) model, and suggested the importance of nonlinear horizontal momentum advection terms in TC genesis. In comparison, *Aiyyer and Molinari* [2003] studied the dynamics of an idealized MRG wave and suggested the importance of its interaction with asymmetric heating in leading to vortex genesis and its poleward movement. A pair of TCs that form successively might eventually turn into twins, appearing as a transition from an MRG wave to an ER wave. However, from a modeling perspective, predicting these TCs is very challenging, because a time lag of 3–5 days in their formation would require a high level of performance in extended-range (beyond 5 days) simulations.

[11] These aforementioned studies collectively indicate the importance of accurately representing the large-scale environmental flows (e.g., tropical waves), realistically resolving mesoscale vortex circulations, simulating the modulation of the large-scale flows on the vortex and the (aggregate) feedback of small-scale processes (e.g., convection) to the vortex. A high-resolution global model that possesses these characteristics is therefore preferred to be adopted to improve the prediction of TC formation. In deference to this view, a global mesoscale model was previously applied [*Shen et al.*, 2010a, 2010b] to address whether and how such a predictive relationship between large-scale flows (explicit or implicit precursor conditions) and hurricane events can be simulated.

Those experiments were performed to investigate the multiple, hierarchical scale interactions and controlling factors that lead to the formation of TC Nargis (2008) and Hurricane Helene (2006). The term multiscale interaction in this study and previous studies [e.g., *Shen et al.*, 2010a, 2010b] is loosely defined as the nonlinear processes that involve flows with different scales, including wavelength reduction of large-scale waves, TC genesis associated with the appearance of a mesoscale vortex, and/or their interaction with resolved or parameterized convective-scale processes. Among the various important physical processes, it was the association with an equatorial Rossby wave and an African easterly wave that were crucial for extending the lead time in the prediction of the genesis of TC Nargis and Hurricane Helene, respectively. Encouraged by these simulations, the original motivation was to examine the model's performance in the simulation of the MJO and its influence on the formation of twin TCs in May 2002, of which the former was one of the major research themes proposed by the Center for Multiscale Modeling of Atmospheric Processes (CMMAP) in 2007. Having recently finished the cases in *Shen et al.* [2010a, 2010b], the current focus will be twin TC formation in association with the ccMRG wave that appeared as the integral of three gyres in the Indian Ocean during the active phase of the MJO in May 2002. Note that the term MRG wave, ccMRG wave, or MRG-type disturbance or even MRG-TD-type disturbance is used interchangeably in this study, and the last one is used for the one which has the phase relationship similar to a forced MRG wave. One specific focus is to understand why such a ccMRG wave is able to determine the timing and location of TC genesis and to help predict TC formation with an extended lead time. The numerical approach is described in section 2, and the results are discussed in section 3. Concluding remarks are given at the end.

2. Data Analysis and Numerical Approach

2.1. Analysis of the MJO, ccMRG Wave and Twin TCs in May 2002

[12] The large-scale MJO associated with the appearance of the twin TCs is shown in the 200-hPa velocity potential (φ) field of the NCEP reanalysis data (Figure 1). The Laplacian of the velocity potential ($\delta^2\varphi/\delta x^2 + \delta^2\varphi/\delta y^2$) represents the divergence of the horizontal winds. The MJO appeared in the Indian Ocean in early May, moved eastward to the West Pacific in mid-May, and weakened in late May [see also *Zhang et al.*, 2007, Figure 3]. On 1 May 2002, the MJO event in the Indian Ocean was indicated by the large-scale organized convection as shown in the METEOSAT 7 IR satellite images (Figure 2a). As the MJO continuously progressed eastward, four TCs (Figures 2b and 2c) subsequently appeared in the Indian Ocean [see also *Moncrieff et al.*, 2007]: TCs Kesiny (or 23S), 01A, 02B, and Errorl. On May 9th, these four TCs appeared as two pairs of twin TCs, "symmetric" with respect to the equator (Figure 2c). However, TCs Kesiny and 01A (the first pair of twin TCs) formed at different longitudes and differed in time by about three days (Figure 2b or Figure 6), one in the SH and the other in the NH. In addition to the two developing systems that became TCs Kesiny and 01, there existed a non-developing system (Figure 2a) during the period 1–7 May prior to the formation of the second twin TCs. These asymmetric and alternating features (the time lag and asymmetry with respect to the equator) suggest the possibility of a ccMRG wave associated with the eastward propagating system (e.g., an MJO in this case). The first three convective systems, which are in association with the gyres S_1, N_1, and S_2 (e.g., Figure 4), provide a very unique case for which to examine the model's performance in simulating both developing and non-developing convective systems that may appear as a ccMRG wave. In contrast, the second pair of twin TCs had a smaller time lag and longitudinal variation in their formation and resembles an equatorial Rossby wave.

[13] The characteristics of an analytic MRG wave solution to shallow water equations on a beta plane are illustrated below, providing a simple way to qualitatively identify a ccMRG wave and trace its evolution in both the global analyses and the model simulations. Figure 3 shows the normalized analytic solutions for a linear MRG wave [*Matsuno*, 1966], which have been well documented in *Wheeler et al.* [2000] and *Kiladis et al.* [2009]. This is similar to Figure 3c in *Kiladis et al.* [2009] with different units. The MRG wave has maximum/minimum meridional wind perturbations at the equator and alternating clockwise and counter-clockwise circulations along the equator (Figure 3a). The high and low geopotential height perturbations in the NH (which are shaded in red and blue, respectively) are in phase with the clockwise and counter-clockwise circulation, respectively. The corresponding geopotential height perturbations in the SH are antisymmetric with respect to those in the NH. Along the direction of the westward propagating wave, the low geopotential height perturbation leads the convergence (indicated by solid green lines) by 1/4 wavelength in the both NH and SH. The unique phase relationship in a free MRG wave is distorted in a forced MRG wave with the inclusion of boundary layer friction [e.g., *Holton*, 1975] and will be discussed later. In this study, the ccMRG wave appeared during an active phase of an MJO that was accompanied by a westerly wind burst (WWB). To identify the MRG wave in the total zonal winds, an idealized WWB solution is superimposed into the zonal wind perturbations (Figure 3b). In addition, Figure 3c shows low geopotential heights (dashed lines) and southerly (red) and northerly winds (blue) winds along the equator. These alternating features of an MRG wave are unique as compared to an ER wave. Figures 3b and 3c are used to examine the wave's evolution in Figures 8 and 9, respectively, in section 3.

[14] To identify the key characteristics of an MRG wave in real data, Figure 4 shows initial horizontal winds and the geo-potential heights at 850 hPa, which are derived from NCEP global analysis and reanalysis at 0000 UTC 1 May 2002. Low geo-potential heights appear over a broad area near the equator between longitudes 65°E∼85°E. Three gyres, each with a closed-form cyclonic circulation, can be identified at this time. These gyres from west to east along longitudes 63°E, 78°E, and 90°E are labeled S_1, N_1, and S_2, respectively. These appeared when the MJO moved eastward (Figures 1 and 2). While the major circulations of both gyres S_1 and N_1 are slightly off from the equator, gyre S_2 is still close to the equator with clear cross equatorial flows. At 500-hPa, gyres corresponding to S_1 and N_1 also appeared at this time (Figure 4b). However, for gyres S_1 and N_1, their vortex circulations at different heights are not vertically

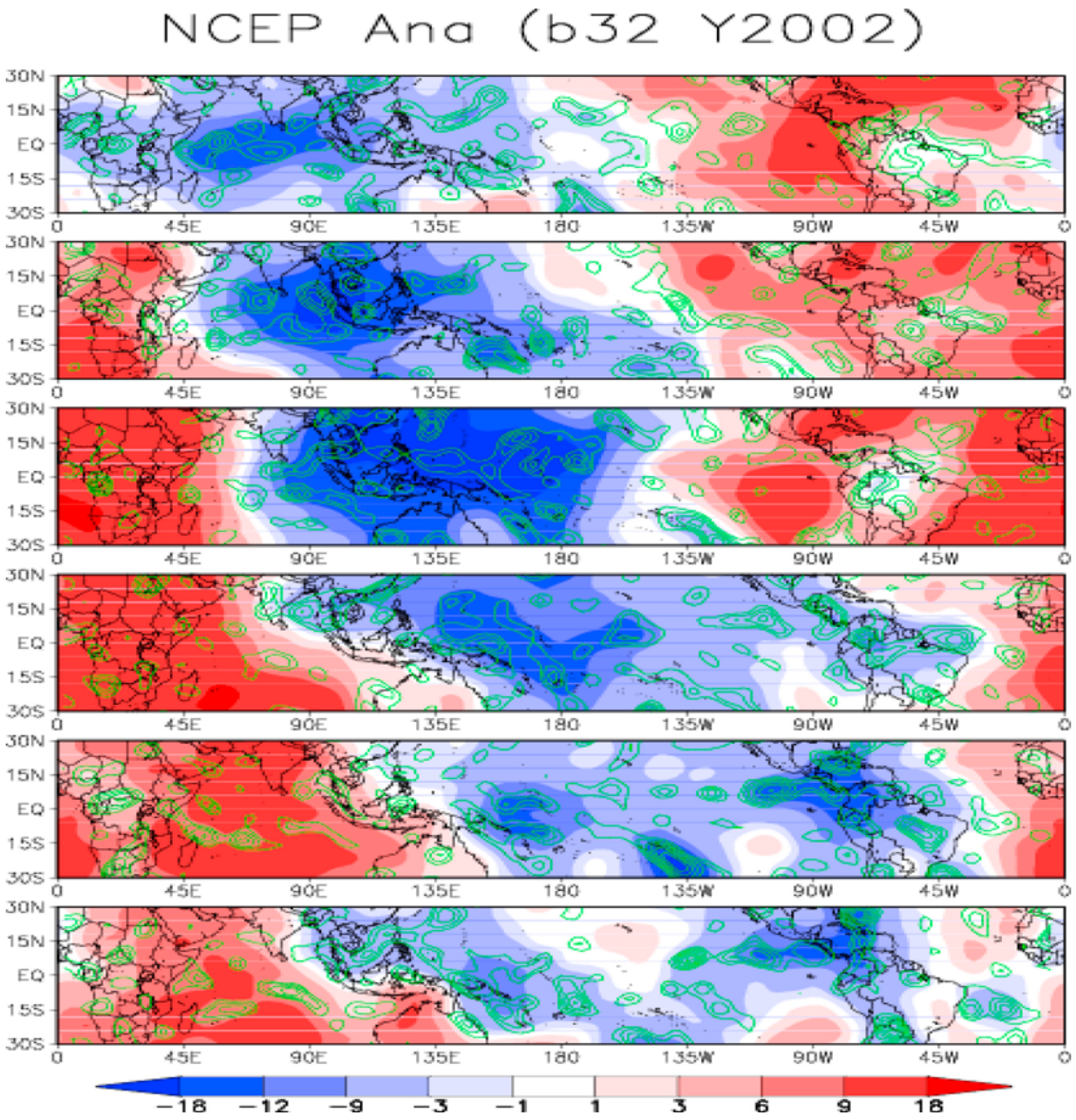

Figure 1. An MJO, which moved eastward out of the Indian Ocean, is shown with NCEP 2.5° reanalysis data. Panels from top to bottom display 200-hPa velocity potential from 2 to 27 May 2002 with a time interval of 5 days.

coherent. This indicates a phase tilt with baroclinicity. In comparison, gyre S_2 is shallow and cannot be detected at 500 hPa at this time. These alternating gyres collectively suggest the appearance of an MRG-type disturbance (or ccMRG wave) with a wavelength that is roughly approximated by the distance between gyres S_1 and S_2. More analyses on the ccMRG wave, including its wavelength, phase speed and vertical structure, are given in the following.

[15] It is important to verify high-resolution global forecasts with global analyses at a comparable resolution. However, due to limits in data availability, NCEP 2.5° (~265 km) reanalyses are still used in some plots (e.g., Figures 1 and 5) to examine the time evolution of weather systems at a time interval of 6 h. Because the spatial resolution in the reanalyses is much coarser than in the analysis (~55 km), the ccMRG wave and the three gyres could be represented differently in the reanalyses. Figure 4c is plotted with the reanalysis data for comparison with Figure 4a. It can be seen that the major differences between these two data sets appear in the representation of the gyres S_1 and S_2 that are associated with the ccMRG wave (near the equator, Figure 4d). This may imply the need for fine grid spacing in the representation of the gyres and ccMRG wave. However, differences in the model physics and/or data assimilation schemes (e.g., the inclusion of high-resolution satellite data), which are associated with the change in grid spacing, could also lead to differences in the representation of the ccMRG wave.

[16] Previous studies suggested that a time-longitude diagram of the meridional winds near the equator [e.g., *Dickinson and Molinari*, 2002] would be useful for the detection of a ccMRG wave's evolution. Figure 5 shows 850-hPa meridional winds averaged over latitude 5°S to 5°N in time-longitude space during the period 1 to 11 May 2002. Note that NCEP "reanalysis" and 10-day model outputs

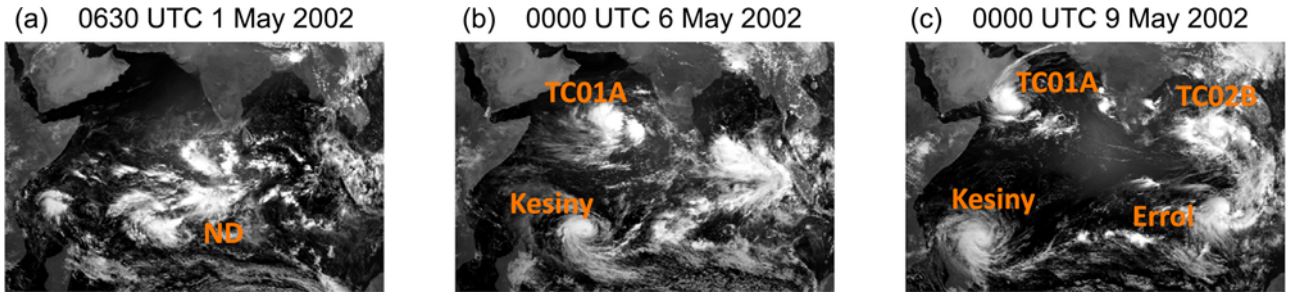

Figure 2. (a) IR data from METEOSAT 7 satellite images show the formation of twin TCs associated with the MJO-organized convection over the Indian Ocean at 0630 UTC 1 May 2002. (b) TCs Kesiny and 01A appear as a pair of twin TCs on May 6; (c) later, a second pair of twin TCs, 02B and Errol, formed on May 9. 'ND' indicates a non-developing system. See also *Moncrieff et al.* [2007].

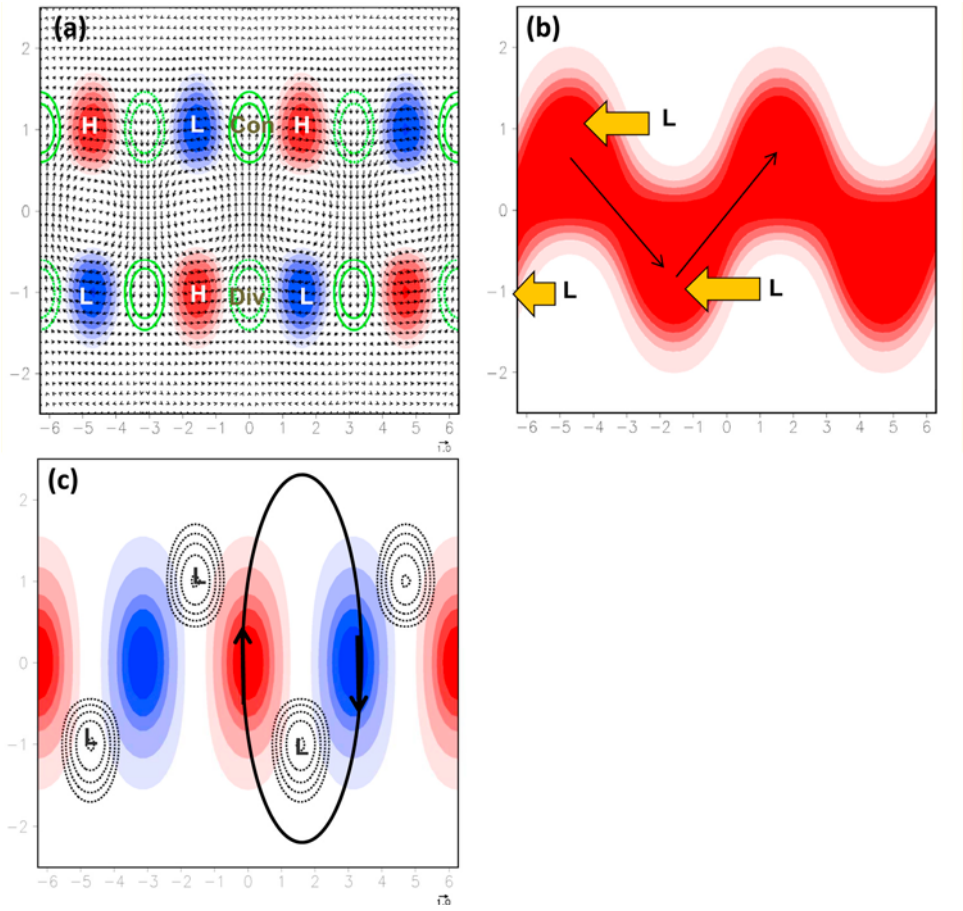

Figure 3. Analytical solutions for a mixed Rossby-gravity wave from shallow water equations on a beta plane. (a) Normalized perturbations of horizontal winds (vectors), geopotential heights (shaded, positive in red and negative in blue), and convergence (contours in green, positive in solid lines and negative in dashed lines). 'H' and 'L' indicate the centers of the maximum and minimum for geopotential height perturbations, respectively. The main features include an asymmetry in the winds and geopotential heights with respect to the equator, cross equatorial flows, and alternating clockwise and counter-clockwise circulations (indicated by the dark line in Figure 3c). The low geopotential heights (shaded in blue) lead the convergence (solid green contour lines) by 1/4 wavelength. (b) A schematic diagram showing the total zonal wind solution, which includes the perturbation zonal winds from the MRG wave, y*sin(x)* EXP ($-0.5*y^2$), and an idealized westerly wind burst (WWB), which is assumed to follow EXP ($-0.5*y^2$). 'L' in Figure 3b still indicates low geopotential heights, which, however, does not take the WWB into consideration. The bold arrows indicate the westward propagation of the MRG wave. (c) Normalized perturbations of meridional winds (shaded) and low geopotential height perturbations (dashed lines).

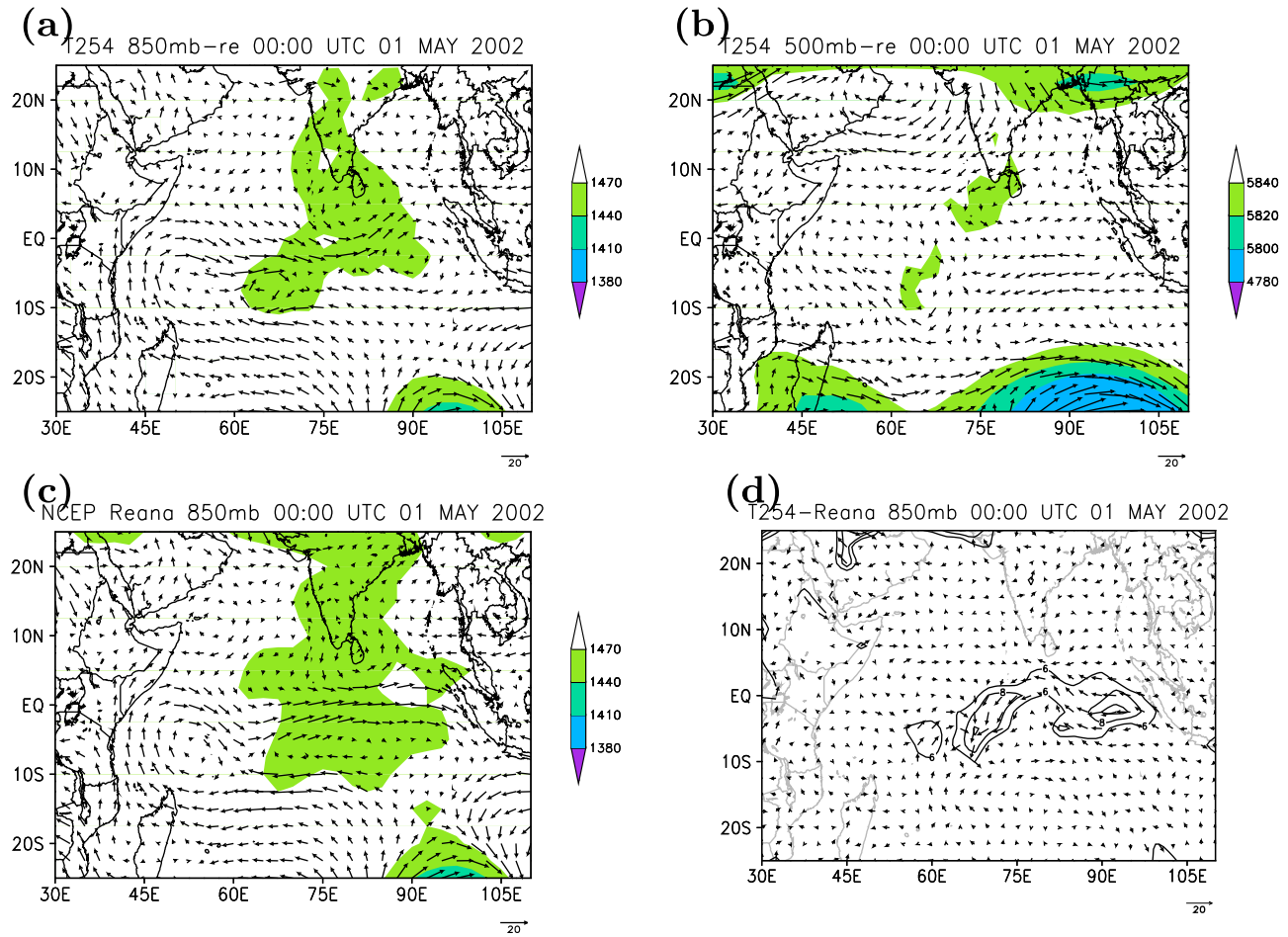

Figure 4. Initial conditions in terms of wind vectors and geopotential heights at (a) 850-hpa and (b) 500-hpa from the NCEP T254 analyses. (c) The same as Figure 4a except for the NCEP 2.5° reanalysis. (d) The difference in 850-hpa winds (vectors) and geopotential heights (with contour lines of 6 and 8) between the NCEP T254 analyses and 2.5° reanalysis. This shows the dependence of the resolved MRG wave.

are displayed. Clearly, the phase speed of the southerly (northerly) winds in red (blue) is westward. The alternating southerly and northerly wind couplets, extending eastward from 50°E, suggest an eastward propagating "group" velocity of ccMRG wave packets or a Kelvin wave in association with the movement of the MJO and a westward propagating ccMRG wave from 90°∼100°E. In this study, the gyres in the SH and NH are labeled as S_n and N_n, respectively. The subscript 'n', either 1 or 2, denotes the appearance of the gyres sequentially from west to east during the transition of the southerly (northerly) winds to northerly (southerly) winds, where areas of strong cyclonic vorticity exist. The period and wavelength of the ccMRG wave are approximately 7∼8 days and 30 degree (wave number 12), respectively. This appears to be a relatively short MRG wave, according to Figure 1 of *Kiladis et al.* [2009]. The corresponding phase speed is roughly equal to the reciprocal of the slope of a constant phase line (the black arrow near the label S2), which is about −1.8 m/s. In the Appendix A, we showed that the estimated phase speed with the wavenumber of 12 is in good agreement with the theoretical value derived from the dispersion relation of the linear MRG wave with an equivalent depth of 90 m and a background zonal wind speed of 3.71 m/s. In Figure 5b, the simulated wavelength and phase speed are compared well with those in the reanalysis. Note that a short MRG wave with comparable wavelength and period was documented in Figure 1b of *Dickinson and Molinari* [2002].

[17] Labels S_1 and N_1 in Figure 5a denote the potential timing and location for the corresponding gyres to develop into tropical cyclones, TC Kesiny and TC 01A, respectively, based on the best tracks. TC 01A appeared to be in association with the intensification of the southerly winds between longitudes 70°∼80°E, a manifestation of the deepening of the ccMRG wave (as also shown in Figure 8). Gyre S_2 along longitude 80°E lasted for more than five days but did not turn into a TC and is also referred as to the non-developing (ND) convective system (see also Figure 2). This provides a good case to test whether the model will produce a false alarm event.

[18] Based on the above discussions, an MRG-type disturbance (or a ccMRG wave) is defined as the integral of the three gyres with the following features: (1) asymmetry with respect to the equator, (2) alternating clockwise and counterclockwise circulations in the SH and NH, (3) cross equatorial

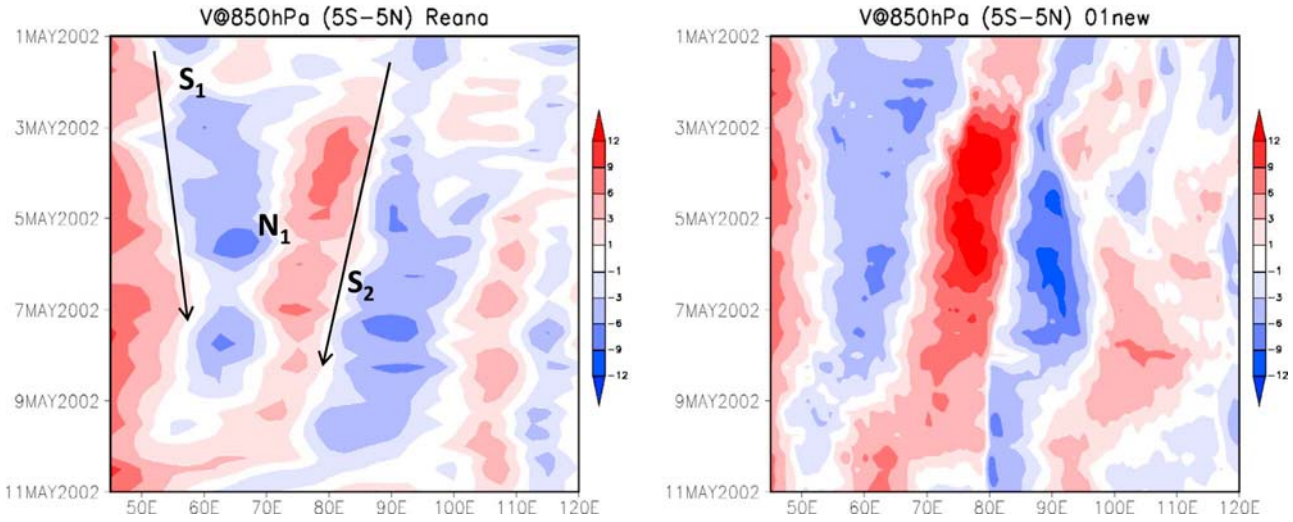

Figure 5. Time-longitude diagrams of meridional winds averaged over latitudes 5°S to 5°N from (a) NCEP 2.5° reanalysis data and (b) the 10-day control run. Southerly (northerly) winds are indicated in red (blue). The westward-propagating disturbances with sloping northerly to southerly flow couplets are likely associated with the MRG wave. Labels 'S_n' and 'N_n' refer to the gyres in the southern and northern hemispheres (SH and NH), respectively, where 'n' is equal to '1' or '2'. S_1 and N_1 roughly indicate the timing and location for the formation of the twin TC Kesiny and 01A, respectively. The latter can be identified clearly by the stronger southerly winds along longitude 75°E between 3 and 5 May. In contrast, S_2 along longitude 80°E is a non-developing convective system. While S_1 seems to move eastward slightly in Figure 5a, this does not change the conclusion that the wavelength is reduced as determined by the distance between S_1 and S_2.

flows (e.g., gyre S_2 along longitude 90°E, and gyre N_1 along longitude 85°E), and (4) phase line tilting with height. In addition, there existed a relatively close match between the estimated phase speed of −1.8 m/s and wavelength of 30° at 850 hPa and the linear MRG wave solution of the shallow water equations. Associating the three gyres with a ccMRG wave will help to examine their evolution as a whole and thus provide an integrated view of their development. Therefore, the accurate representation of an initial ccMRG wave and its evolution (in terms of its phase and amplitude) are useful for the detection of TC genesis.

2.2. Numerical Approach

[19] The GMM, previously called the high-resolution finite-volume GCM (fvGCM), is composed of three major components: (1) finite-volume dynamics, (2) NCAR CCM3 physics, and (3) the NCAR Community Land model [*Lin et al.*, 2003; *Lin*, 2004; *Atlas et al.*, 2005; *Shen et al.*, 2006a]. After the NASA Columbia supercomputer came into operation in late 2004 [*Biswas et al.*, 2007], a global mesoscale model (GMM) with a high resolution of 1/12 degree (∼9 km at the equator and 6.5 km at middle latitudes) was successfully deployed in 2005. Prior to the deployment of the 1/12 degree GMM, a 1/2 degree model was first tested systematically with hundreds of 5-day NWP (numerical weather prediction) runs in 2002 [*Lin et al.*, 2003], and a 1/4 degree model was applied to the forecasting of hurricanes in 2002 and 2004 [*Atlas et al.*, 2005]. The 1/4 degree model doubled the resolution of many operational global weather models in 2004. Later, a 1/8th degree GMM was deployed to illustrate the impact of increased resolution on the simulation of three intense hurricanes from 2004 and two terrain-induced mesoscale eddies [*Shen et al.*, 2006a]. With the 1/8th degree model, *Shen et al.* [2006b] examined the impact of explicitly resolved moist processes (i.e., no CPs) as well as increased resolution on 5-day forecasts of Hurricane Katrina's (2005) track, intensity and near-eye wind distribution, and *Shen et al.* [2006c] documented more than sixty 5-day forecasts of intense hurricanes from 2004 and 2005. The model includes a hybrid sigma-pressure vertical coordinate; the vertical resolution has 18, 32, 48, 55, and 64 layers implemented with differing model tops of 2.9, 0.4, 0.4, 0.01, 0.01 hPa, respectively. In this study, 32 layers with a domain top of 0.4 hPa are used.

[20] Dynamic initial conditions (ICs) and sea surface temperatures (SSTs) are derived from GFS T254 (∼55 km) analysis data and 1° optimum interpolation SSTs from the National Centers for Environmental Prediction (NCEP). No vortex initialization (e.g., a bogus vortex) is applied in the initial fields. For model verification, NCEP T254 (∼55 km) analyses and/or NCEP 2.5° reanalysis data are used. Though the T254 analyses data are better for model verification because of a much finer resolution, these analyses were archived only at 0000 UTC. In contrast, the NCEP 2.5° reanalyses are available at a time interval of 6 h from a public ftp site. Best tracks for the TCs are available from the Joint Typhoon Warning Center (JTWC) and are used for comparison. QuikSCAT seawinds data [e.g., *Liu et al.*, 1998], available at a 0.5° resolution, are also used for verification of the low-level (surface) winds. Precipitation from the Tropical Rainfall Measuring Mission (TRMM) [*Huffman et al.*, 2007] is also used for verification.

Table 1. Numerical Experiments and Their Modeling Configurations[a]

EXP ID	IC	Grid-Scale Condensation	CPs	Remarks
CNTL	05/01	yes	no	
EXP-A	05/01	yes	ZF95 and H94	
EXP-B	05/01	yes	NCEP SAS	
EXP-C	05/01	yes	ZF95 and H94 except for a global channel	No CPs in the global channel 0°–40°N
EXP-D	05/01	yes	ZF95 and H94 except for a global channel	No CPs in the global channel 40°–0°S.
EXP-E	05/02	yes	no	The same as the control run with a different set of ICs.

[a]EXP ID is the name of the experiment; IC is the starting date of the initial conditions. Grid-Scale and CPs indicate the usage of an explicit grid-scale condensation scheme and/or cumulus parameterizations (CPs). Dates are given as month/day.

[21] In order to make the model suitable and feasible for studying TC climate, the focus is on the model's performance regarding TC genesis rather than its ability to simulate very fine-scale "convective" processes such as vortical hot towers. The control run in this study, which is a 10-day forecast initialized at 0000 UTC 1 May 2002, is performed at 1/4 degree resolution using only a grid-scale condensation scheme [*Sundqvist*, 1988] (i.e., no CPs). The same model configuration was previously used for 7-day simulations to examine the hierarchical multiscale interactions (e.g., the excitation of an equatorial Rossby wave that may lead to the formation of TC Nargis (2008) in the Indian Ocean [*Shen et al.*, 2010a]). This model also realistically simulated the successive initiation of multiple (six) AEWs and the association of the 4th AEW with hurricane formation (e.g., Hurricane Helene, 2006) in 30-day experiments initialized at 0000 UTC 22 August 2006 [*Shen et al.*, 2010b]. These studies, among others that are being conducted, suggest that the model configurations are able to realistically simulate the large-scale environmental flows (e.g., equatorial Rossby waves and AEWs), their time-varying evolution, and their modulation of TC formation with reasonable results. This also suggests a potential for extending the lead time for TC genesis prediction. In this study, the model's ability to simulate the evolution of the ccMRG in early May 2002 and the successive formation of two TCs, that later turned into twin TCs, is further examined.

[22] As discussed in the Introduction, previous studies suggested that tropical waves (e.g., MRG waves) and TCs could be modulated by moist processes; thus, realistic representation of the moist processes in numerical models appears crucial for simulating the scale interactions that lead to tropical cyclogenesis. To verify whether the simulations of the ccMRG wave and TCs (and gyres as well) are sensitive to the choice of particular model moist physics, parallel experiments are performed with the same initial conditions but different CPs. The first experiment (labeled "EXP-A") follows the settings in the control run but applies the *Zhang and McFarlane* [1995] (denoted as ZM95 hereafter) and *Hack* [1994] (denoted as H94 hereafter) schemes for deep and shallow-and-midlevel convection, respectively. This configuration was previously used in *Atlas et al.* [2005]. The second experiment (labeled "EXP-B") is performed with the NCEP SAS (simplified Arakawa and Schubert) scheme [*Pan and Wu*, 1995]. The impact of regional changes in the moist processes is examined by comparing the control run, EXP-A run, and two additional runs (EXP-C and EXP-D), which disable CPs only in a global channel (e.g., from the equator to 40°N or from 40°S to the equator) and enable the ZM95 and H94 schemes elsewhere. All of these runs are used to examine the association of the simulated ccMRG wave with the timing and location of twin TC formation as well as a false-positive event that appears as the over-intensification of the gyre S_2. An additional run (EXP-E) initialized at 0000 UTC 2 May 2002 was performed to illustrate the sensitivities of simulations to a different set of initial conditions (ICs). Table 1 gives a summary of these six experiments.

3. Results

[23] In the following sections, simulations of twin TC genesis and its association with a ccMRG wave using the GMM initialized with NCEP T254 analysis data at 0000 UTC 1 May 2002 are discussed. To our knowledge, this is the first such attempt at a global simulation of twin TC genesis and one non-developing system with real-data. The evolution of the simulated ccMRG wave is verified against NCEP analyses in section 3.1. The simulated TC tracks and intensities in the 10-day control run are compared with the best track observations in section 3.2. In section 3.3, the sensitivity of the ccMRG wave and TC simulations to different moist processes are discussed as is the simulated precipitation associated with each of the developing and non-developing systems (gyres S_1, N_1 and S_2) on a regional scale. At the end of section 3.3, the sensitivity of the simulations to a different set of ICs is examined. Then, a conceptual diagram is proposed to illustrate the scale interactions of the three gyres.

3.1. Evolution of the ccMRG Wave and Its Impact on the Formation of the Twin TCs

[24] Figure 6 shows the evolution of 850-hPa winds and geopotential heights from the GMM control run after 48, 72, and 96 h of integration and their corresponding fields from the NCEP analyses. The NCEP data shows that near the center in each of the gyres S_1 and N_1, the low continues to deepen. As time progresses, the wavelength of the ccMRG wave shortens as indicated by the reduced distances between gyres S_1 and S_2 (Figures 6a, 6c, and 6e). Note that gyre S_2 (e.g., the gray oval in Figure 6c) resembles a linear MRG wave packet (Figure 3c) well. Gyre N_1 moved northward on May 5 (Figure 6c), and later developed into TC 01A on May 6. At 0000 UTC 5 May, the centers of gyre N_1 at 850 hPa (Figure 6e) and 500 hPa (Figure 7a) are still not vertically coherent. These features revealed in the analyses are simulated quite well by the model (Figures 6b, 6d, 6f, and 7b). During this period, the GMM control run also reproduces a realistic evolution of Gyre S_1, which later developed into TC Kesiny, and slightly overestimated Gyre S_2, which, however, did not develop into a TC.

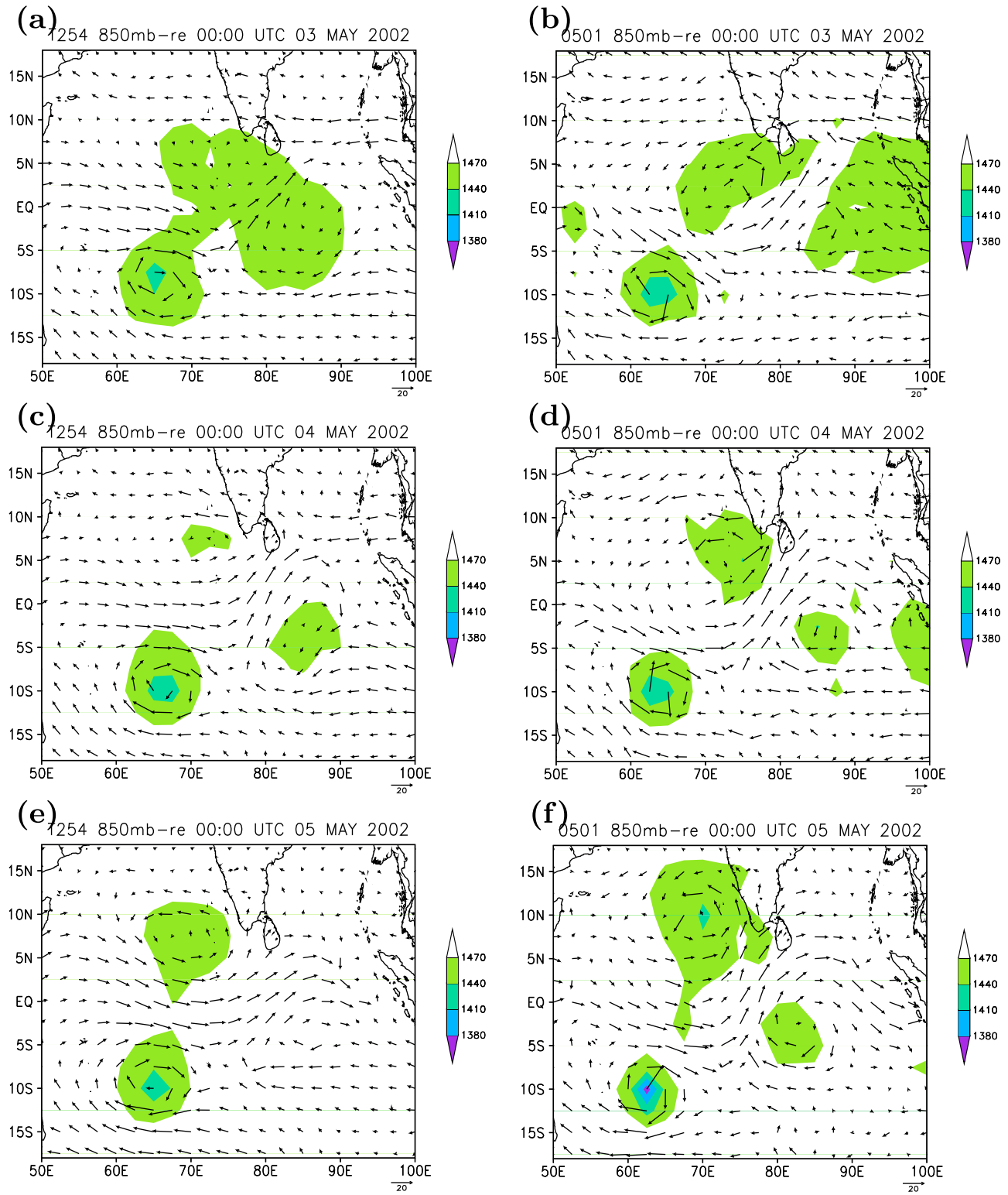

Figure 6. The 850-hPa winds (vectors) and geo-potential heights (shaded) at 0000 UTC 3–5 May 2002 from (a, c, and e) NCEP T254 analyses and (b, d, and f) the control run. There were three gyres with cyclonic circulation centers, S1 N1 and S2. A reduction in the MRG wavelength can be seen by the reduced distance between gyres S1 and S2. During the period of MRG wave intensification, the northern vortex moved poleward in association with a northward extension of the MRG wave and later developed into TC 01A. The gray oval in Figure 6c indicates the circulation of gyre S2 which is similar to that of a MRG wave in Figure 3c.

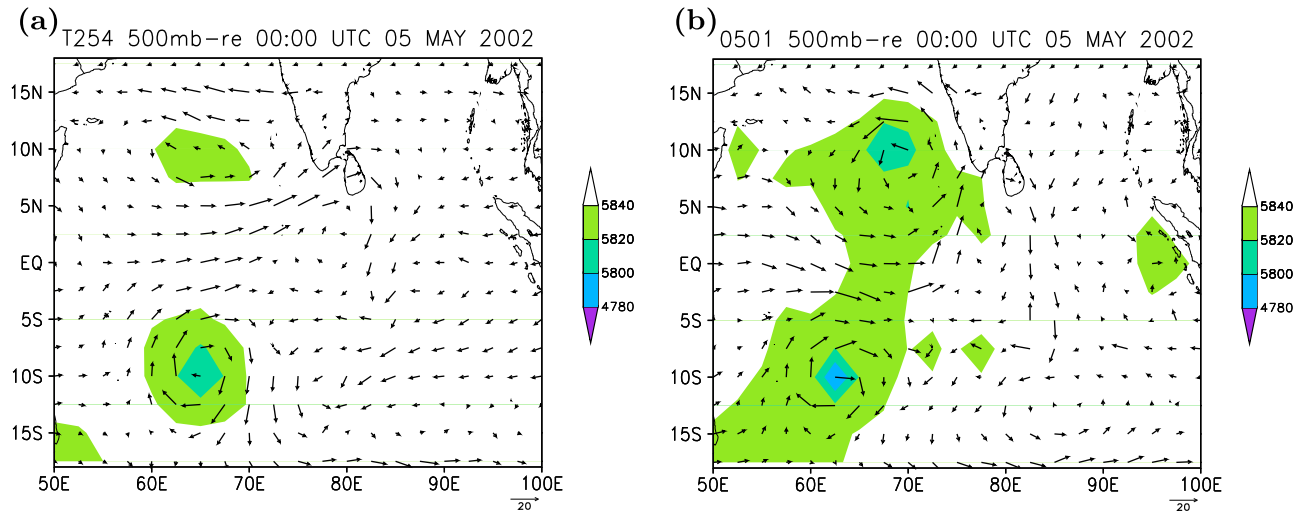

Figure 7. The 500-hpa wind vectors and geo-potential heights at 0000 UTC 5 May 2002 from (a) the NCEP T254 analysis and (b) the control run.

[25] Figure 8 provides a qualitative but simple view of the intensification of the ccMRG wave and the northward movement of Gyre N_1 during the period 1–5 May. These can be seen in 850-hPa zonal winds from NCEP T254 analyses that became wavy, deepened, and extended poleward (Figures 8a, 8b, and 8c). The deepening in zonal winds between longitudes of 72°E∼82°E is consistent with the intensifying southerly winds (e.g., Figure 5). The control run reasonably simulated the intensification and poleward extension of the ccMRG wave associated with the

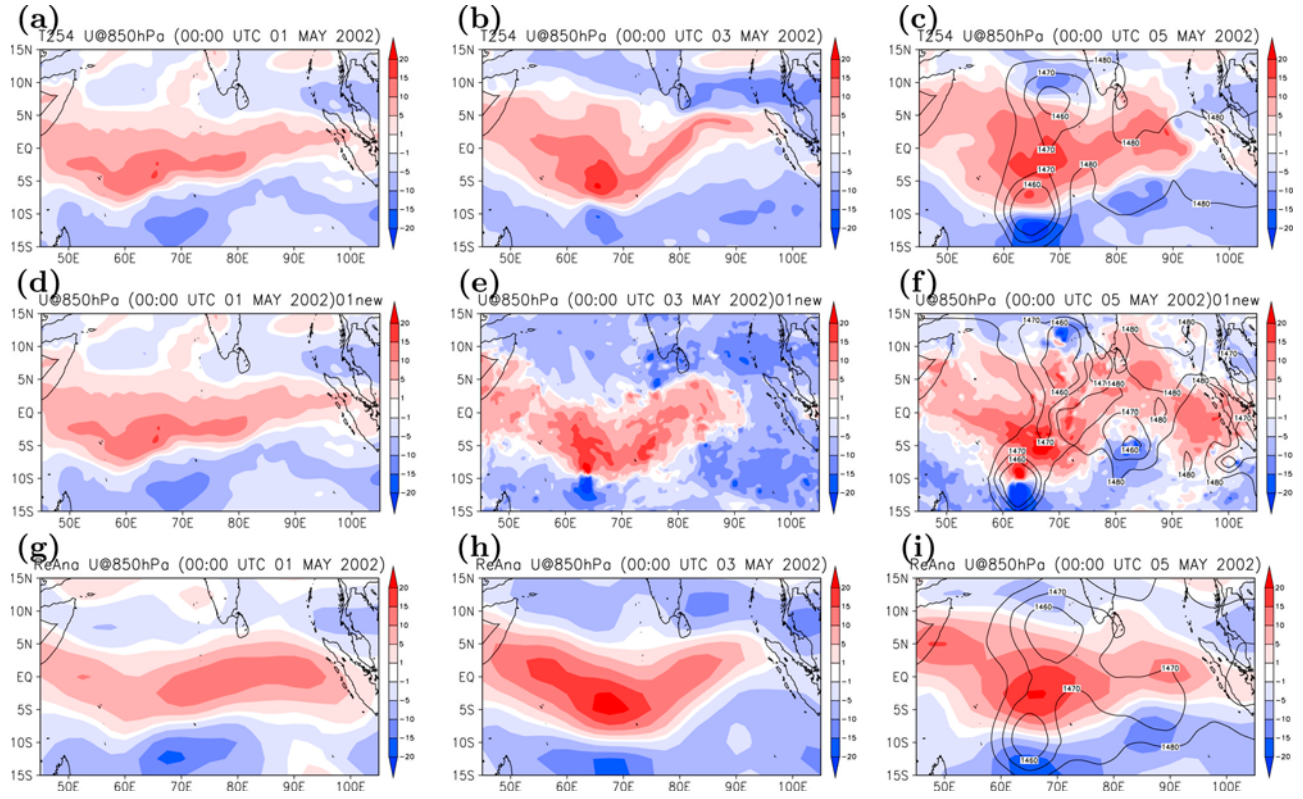

Figure 8. Evolution of 850-hPa zonal winds (shaded) and geopotential heights (contours) from (a, b, and c) NCEP T254 analyses, (d, e, and f) the control run and (g, h, and i) NCEP 2.5° reanalyses at 0000 UTC 1 May (Figures 8a, 8d, and 8g), the initial time, 0000 UTC 3 May (Figures 8b, 8e, and 8h) and 0000 UTC 5 May (Figures 8c, 8f, and 8i). Selected contour lines of geopotential heights include 1460, 1470 and 1480 m. As time progresses, zonal winds become wavy, deepen, and extended poleward. The pattern in Figure 8f is similar to the idealized solution in Figure 3b.

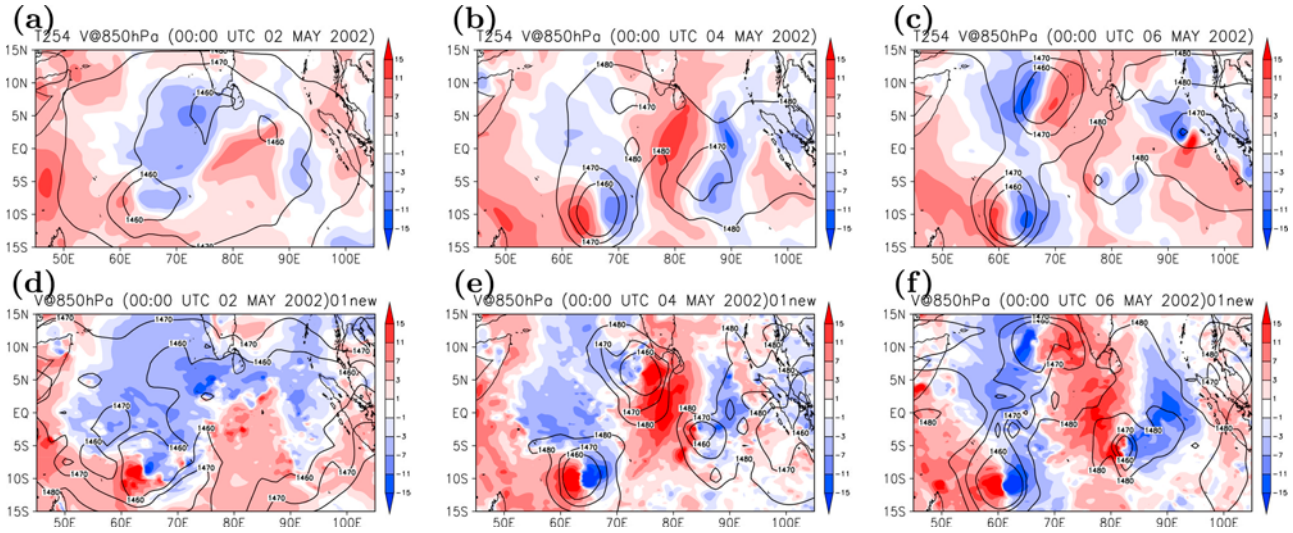

Figure 9. The evolution of the MRG wave and its relation to the formation of TCs Kesiny and 01A. Meridional winds (shaded) and geopotential heights (contours) on (a) 2, (b) 4 and (c) 6 May 2002 from NCEP T254 analyses. (d, e, and f) As for Figures 9a, 9b, and 9c, but from the GMM control run. The MRG wave is associated with the northerly/southerly wind couplets and low geopotential heights, the latter of which may be associated with the development of a TC. Selected contour lines of geopotential heights include 1460, 1470 and 1480 m. The pattern in Figures 9b, 9c, 9e, and 9f is similar to the linear MRG wave in Figure 3c.

three gyres (Figure 8d, 8e, and 8f; more details on the convective activity are revealed in the GMM results than in the analysis data). However, the wave packet associated with the simulated ccMRG wave moved eastward faster than that in the global analyses. Figures 8g, 8h, and 8i show the corresponding fields from the NCEP 2.5° reanalysis data for comparison, suggesting a similar tendency of ccMRG wave evolution with comparable intensity. The ccMRG wave in Figure 8f or 8i resembles the linear MRG wave in Figure 3b.

[26] To facilitate the discussion of the sensitivity experiments in section 3.4, the 850-hPa meridional winds and geopotential heights are analyzed to examine the evolution and propagation of the ccMRG wave and its relation to the formation of TCs Kesiny and 01A in Figure 9. A similar representation of the linear MRG wave was shown in Figure 3c. Figure 9 shows the NCEP T254 analyses (Figures 9a, 9b, and 9c) and the control run (Figures 9d, 9e, and 9f) at 0000 UTC 2, 4, and 6 May 2002. The westward-moving ccMRG wave is indicated by the alternating southerly and northerly wind couplets and three accompanying gyres located between the transitions from southerly to northerly winds. In the early stage, the wavelength of the ccMRG wave reduced in association with the faster westward speed of gyre S_2 compared to that of gyre S_1. At the same time, the ccMRG wave was deepening and extended northward into the NH (also see Figure 8f) as indicated by the intensifying southerly winds (Figures 9b and 9e). Accordingly, one may conclude that gyre N_1 continued to develop in association with the deepening of the ccMRG wave, gradually moving northward with the wave's northward extension before intensifying and developing into a TC. In section 3.3, a similar analysis is made for the sensitivity experiments.

[27] The vertical structure of the ccMRG wave at 0000 UTC 4 May 2002 is shown in the vertical cross sections of the meridional winds in Figure 10. Figures 10a and 10b display the meridional winds in the NCEP T254 analyses averaged over latitudes 5°S to the equator and from the equator to 5°N, respectively. Figures 10c and 10d show the corresponding meridional winds from the model simulations. Notable features include down-shear tilting of the ccMRG phase lines, which suggests an upward propagating transfer of energy. Note that there are westerly winds at low levels and easterly winds at upper levels, giving an easterly wind shear. These features resemble those of the MRG wave in Figure 3 of *Dickinson and Molinari* [2002]. The location of the gyre S_2 (N_2) is roughly indicated by the transition of the southerly (northerly) winds to northerly (southerly) winds in Figure 10a (Figure 10b). At this time, the main circulation of Gyre S_1 was already away from latitude 5°S. Though the phase line tilting is an important feature of the ccMRG wave, the accompanying vertical shear is unfavorable for TC formation. Thus, it is important to determine when the vertical shear might be reduced to favor TC formation. This will be discussed along with TC 01A below.

[28] Figures 11 and 12 display latitude-height cross sections of zonal winds averaged over 4° longitudes centered on the gyre N_1 at 850 hPa (Figures 11a–11c and 12a–12c) and the corresponding meridional winds averaged over 4° latitudes (Figures 11d–11f and 12e–12f). NCEP analyses at 0000 UTC 5, 6 and 7 May are shown in Figure 11, respectively, while the model simulations at the corresponding times are shown in Figure 12. Figures 11a, 11b, and 11c show low- and mid-level westerly winds (in red) in low latitudes (0°∼8°N) up to 400 hPa, and easterly winds (in blue) to the north of the westerly winds. Figures 11d, 11e, and 11f show low- and mid-level northerly winds (in blue) on the west side and southerly winds (in red) on the east wide. Zero zonal wind speeds are indicated in white. These figures indicate clearly the low- and mid-level cyclonic circulations (CCs). Overall, the tilted phase line of zero wind

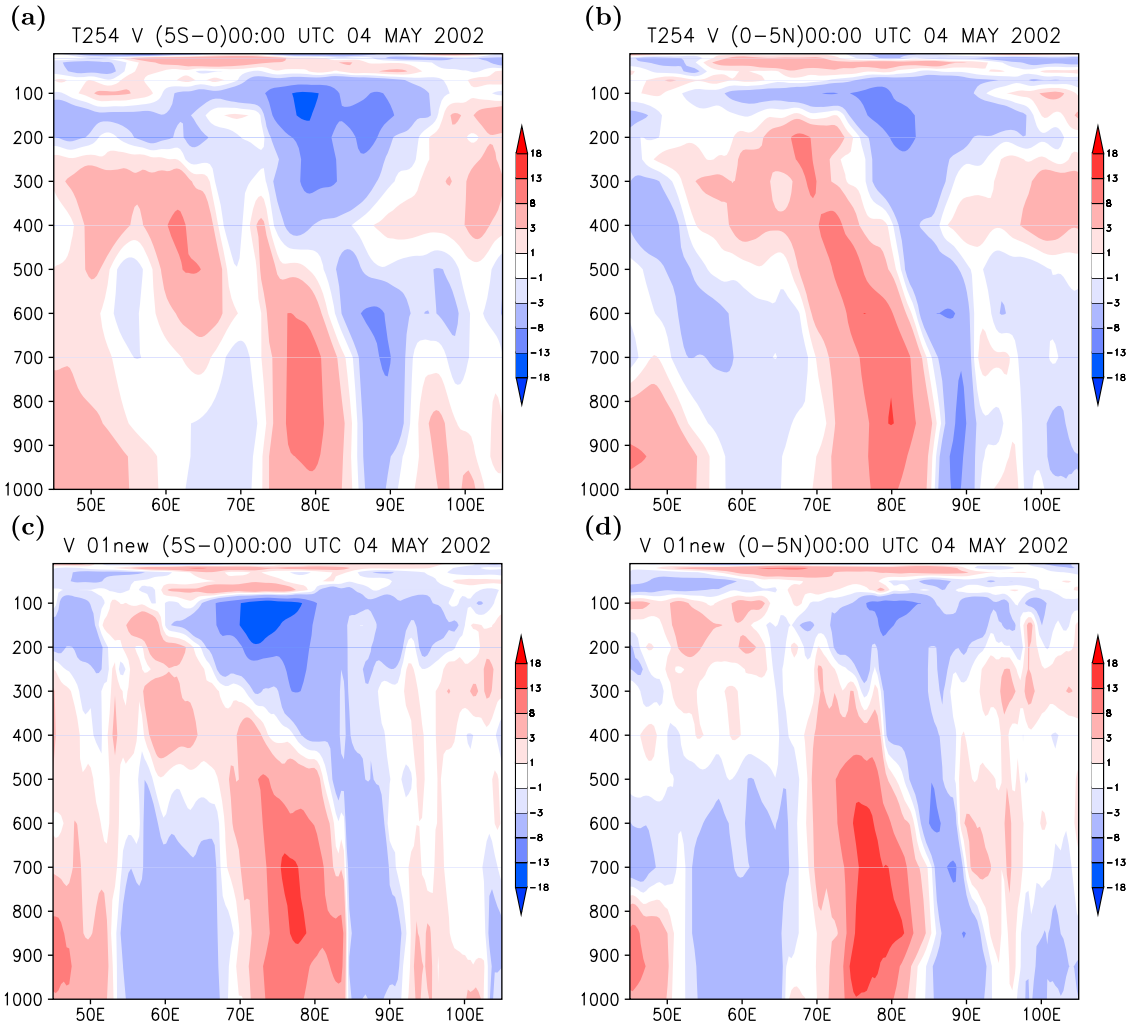

Figure 10. Longitude-height cross sessions of meridional winds at 0000 UTC 4 May 2002 averaged over latitudes (a and c) 5°S to the equator and (b and d) from the equator to 5°N. Figures 10a and 10b show the NCEP T254 analyses while Figures 10c and 10d show the control run. S2 and N1 roughly indicated the location of the gyres.

speeds at the earlier time indicates the vertical shear near the center of the CC (e.g., Figures 11a and 11d). As time proceeds, the CC moves westward and northward, and the phase line of zero wind speeds near the center of the CC becomes upright, indicating smaller vertical shear. Thus, the coherence of the CC centers at different heights becomes favorable for TC formation. Overall, the structure and evolution of the CC associated with the gyre N_1 are realistically simulated by the GMM control run. On May 6 when TC01A formed, the 200–850 hPa vertical shear appeared anti-cyclonic (AC) centered at the minimum of sea level pressure where wind shear was weak (less than 10 m/s) (not shown). The anti-cyclonic wind shear is associated with a low-level CC (at 850 hPa) and an upper-level AC (at 200 hPa). Although the centers of the low-level CC and upper-level AC were not vertically coherent at this time, the appearance of the AC vertical shear near the low pressure center is consistent with the findings by *Shen et al.* [2010a], who examined the formation of Nargis (2008). However, the simulated TC 01A appears at 68°E and 11°N on May 6, which is about 2.5° north of the observed TC 01A.

[29] As discussed in section 1, the phase lag of the meridional winds and convergence/divergence may serve as an indicator of whether the wave disturbance resembles a MRG-type disturbance or a TD-type disturbance; the latter indicates the impact of other processes such as boundary layer friction on the distortion of the phase relationship. While the sensitivities of the simulations to the boundary layer processes are being performed with a focus on the impact of the boundary layer heights (which are a function of the Richardson number), in this study, the phase lag of the two fields at different heights are simply compared. Figure 13 shows a Hovmoller diagram of the vertical pressure velocity (shaded) and meridional winds (contours) averaged over latitudes 0 to 5°N at 850-hPa (Figure 13a) and 500-hPa (Figure 13b). Since the model is hydrostatic, the vertical pressure velocity is a good indicator of the horizontal convergence/divergence. The maximum vertical pressure

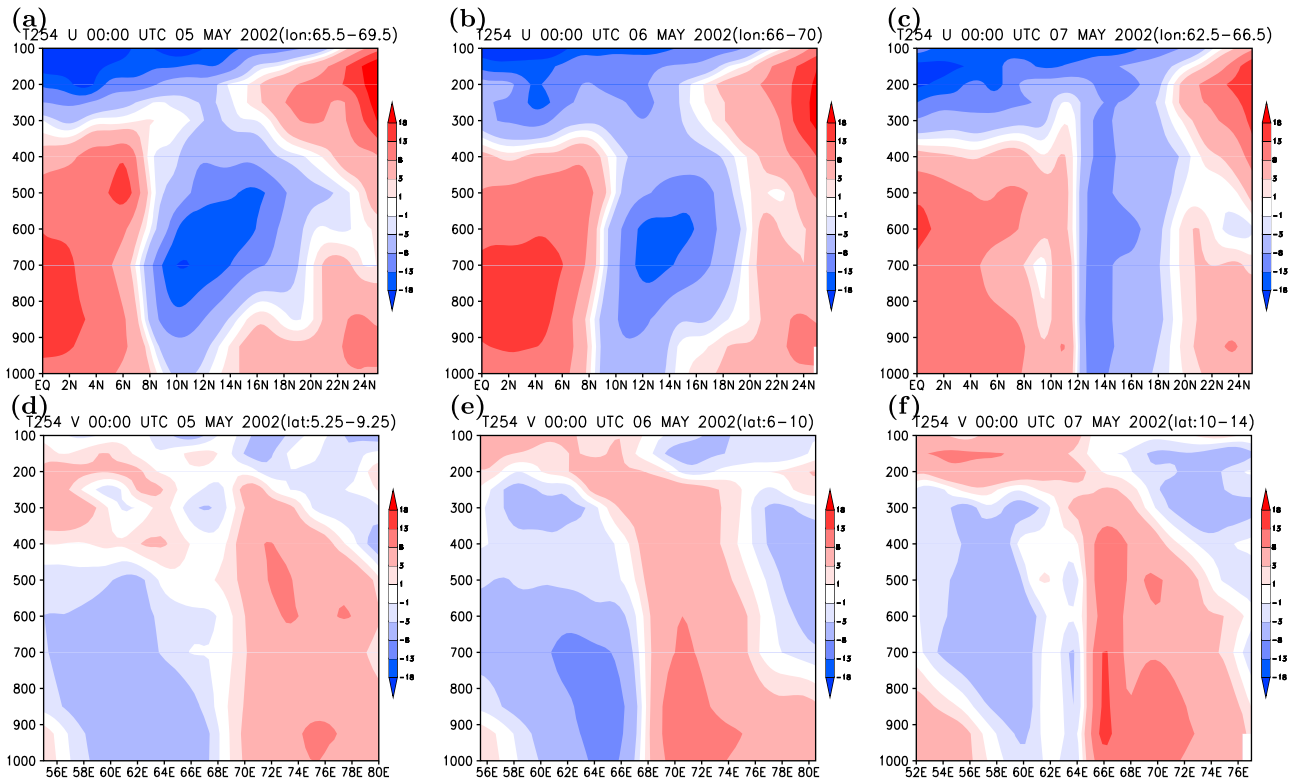

Figure 11. (a, b, and c) Latitude-height cross sections of zonal winds averaged over 4° longitudes centered on the gyre N1 and (d, e, and f) longitude-height cross sections of meridional winds averaged over 4° latitudes. Mid- and low-level cyclonic circulations near the center of the gyre N1 from the NCEP 254 analyses validated at 0000 UTC 5 (Figures 11a and 11d), 6 (Figures 11b and 11e), and 7 (Figures 11c and 11f) May 2002.

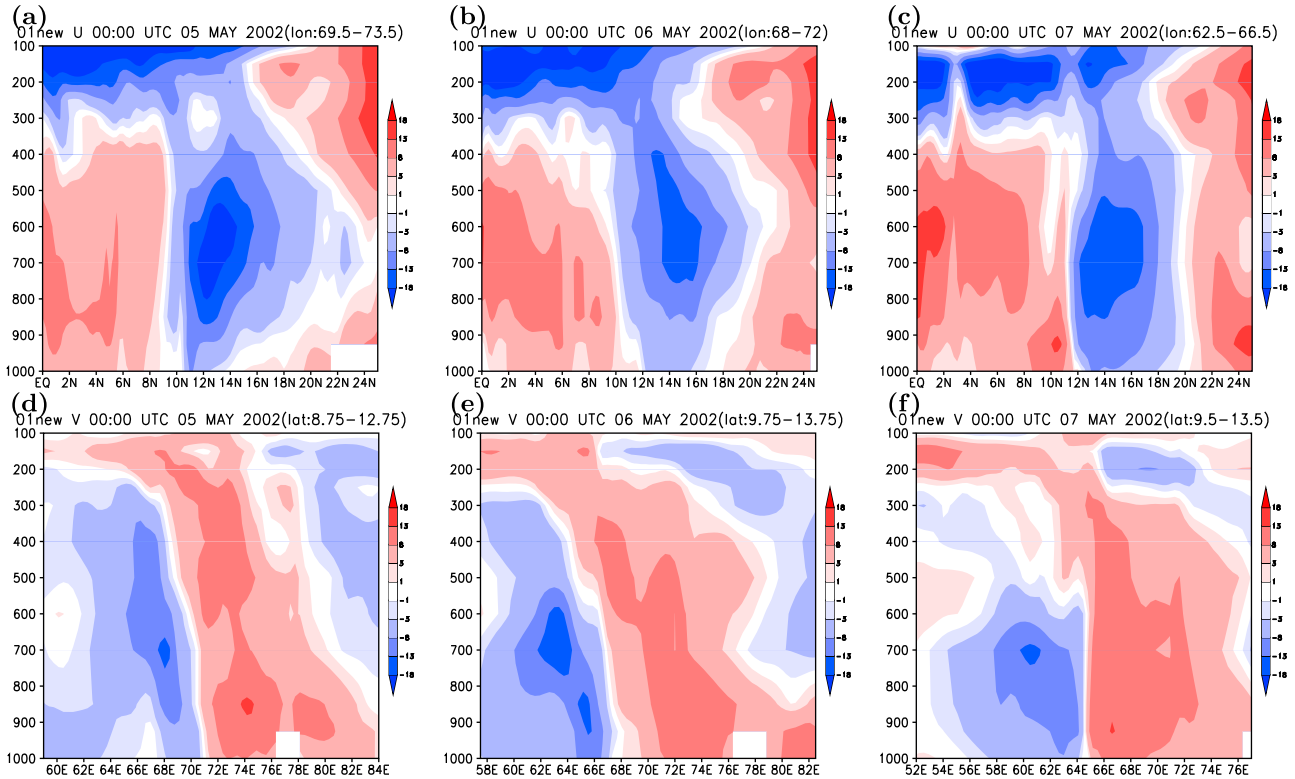

Figure 12. Same as Figure 11 but from the GMM control run.

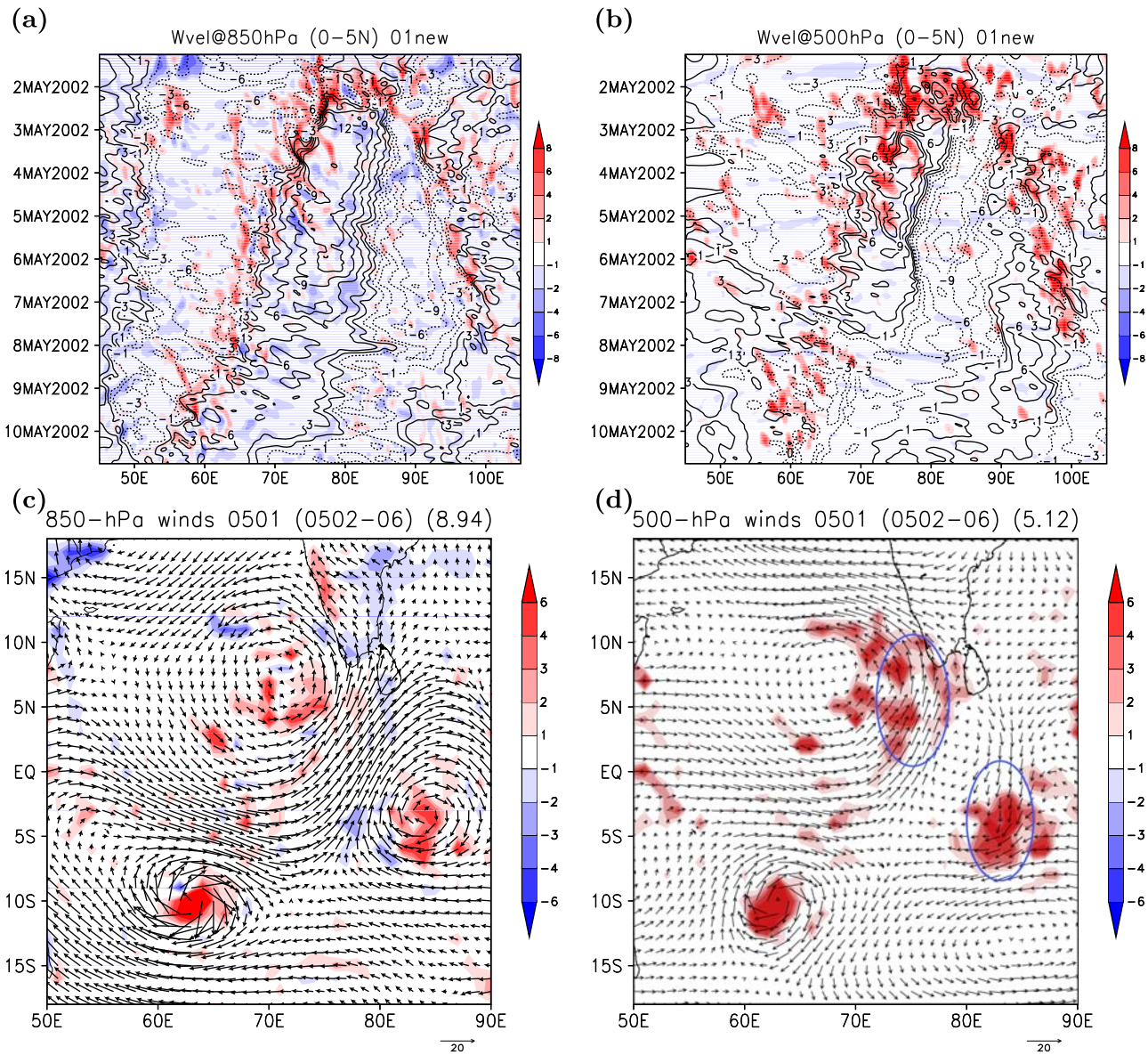

Figure 13. Phase relationship between horizontal winds (m/s) and vertical pressure velocity (shaded, -1×10^{-1} Pa/s). Hovmoller diagram of vertical velocity and meridional winds (contours) averaged over latitudes 0 to 5°N at (a) 850 hPa and (b) 500 hPa. The 850-hPa vertical velocity maximum, which roughly leads the southerly wind maximum by 1/4 wavelength in the westward direction, is in phase with the center of the gyre N1 as indicated by the zero meridional winds. In contrast, the 500-hPa vertical velocity maximum from 2 to 6 May, which is roughly in phase with the southerly wind maximum, is behind the center of the gyre N1 by 1/4 wavelength. The (c) 850-hPa and (d) 500-hPa horizontal winds and vertical velocity averaged over 0000 May 2–7, 2002.

velocity at 850 hPa is in phase with zero meridional winds, suggesting the vertical pressure velocity roughly leads the southerly wind maximum by 1/4 wavelength in the westward direction. In contrast, the vertical pressure velocity maximum at 500-hPa is in phase with the southerly wind maximum before May 5, which is consistent with the linear free MRG wave in Figure 3a. This suggests that the westward propagating signals at 500-hPa has the phase relationship similar to that of a free MRG wave mode, while the corresponding signal at low levels (850-hPa) has the phase relationship close to that of a "forced" MRG wave mode that is assumed to be influenced by boundary layer processes. Note that because the model includes (relatively) comprehensive physical parameterizations, other low-level processes such as shallow convection may also play an important role in the distortion of the phase lag. While Figures 13a and 13b show the combined features of the gyres N_1 and S_1 between latitudes 0–5°, Figures 13c and 13d are plotted to show the phase relationship of vortex center and vertical motions for individual gyres at 850 and 500 hPa, respectively. From

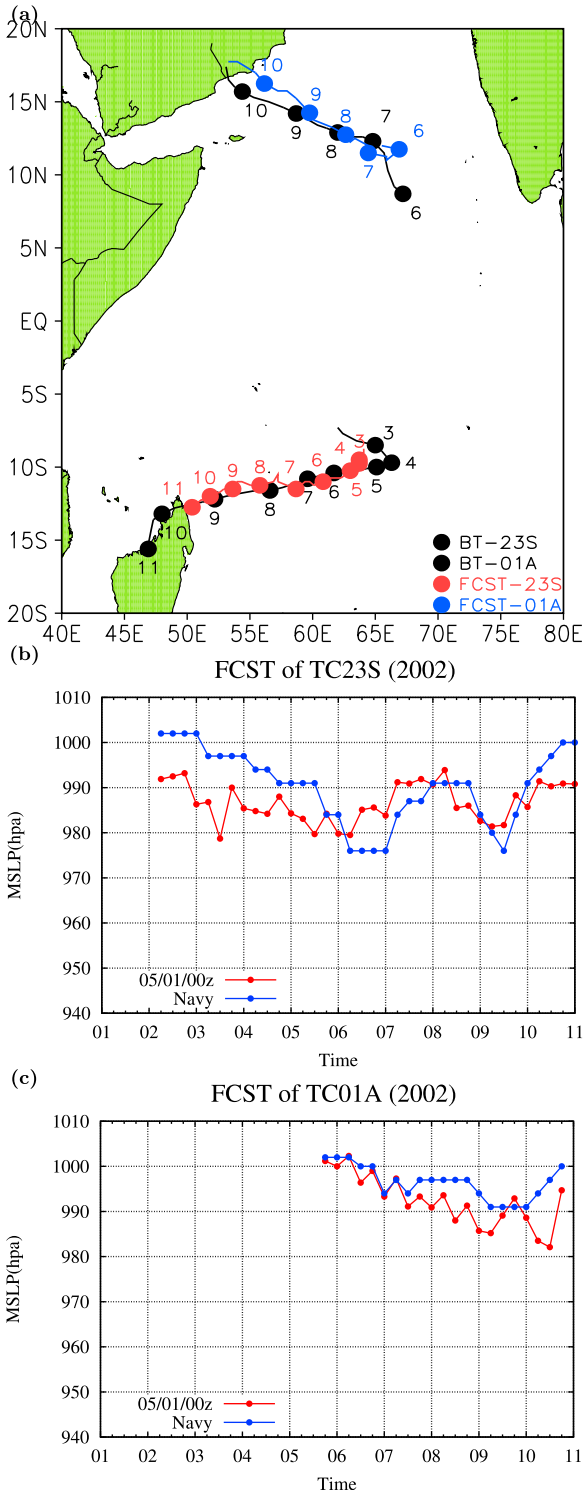

Figure 14. (a) Track and (b) intensity simulations of TCs Kesiny and (c) 01A from the 10-day control run initialized at 0000 UTC 1 May 2002. In Figure 14a, black lines indicate the best track, a blue (red) line indicates the simulated track of TC Kesiny (TC 01A). In Figures 14b and 14c, a blue line indicates the intensity of best track, while a red line is the simulated intensity.

Figure 13c, it is very clear that vertical motions at 850 hPa appear mainly near the vortex center of gyres S1 and S2. The phase relationship is similar to that of a TD-type disturbance. In contrast, vertical motions at 500 hPa are in phase with southerly winds in the NH and with northerly winds in the SH, which are shown in blue ovals of Figure 13d. All of these above suggest a transition from a MRG-type disturbance (e.g., gyre N_1) to a TD-type disturbance.

3.2. Simulated Tracks and Intensities for Twin TCs Kesiny and 01A

[30] The TC Formation Alert for Kesiny (2002) in the SH was issued (re-issued) at 2100 UTC 2 (0600 UTC 3) May, as shown in the best track of Figure 14a. Once formed, TC Kesiny first moved eastward, before turning southward, and finally west-southwestward. By 0600 UTC 6 May, Kesiny's MSLP (minimum sea level pressure) deepened to 976 hPa, and maintained that strength until 0000 UTC 7 May (Figure 14b). It continued to move west-southwestward and crossed the northern tip of Madagascar on 9 May. The accompanying torrential rains caused severe and widespread flooding in Madagascar. About 520,000 people were adversely affected by Kesiny and 5000 were left homeless. TC 01A, Kesiny's counterpart in the NH, was first recorded at 1800 UTC 5 May (Figure 14c), about three days after Kesiny's alert was issued, and moved northwestward due to the influence of a sub-tropical ridge to its north. It made landfall near Salalah, Oman at about 0900 UTC 10 May and then weakened afterward. TC 01A was the first storm to hit Salalah in nearly 20 years and caused substantial damage (http://www.australiasevereweather.com/cyclones/2002/summ0205.htm). Based on the *World Meteorological Organization* (*WMO*) [2004] report that summarized the track prediction of TC 01A in the Arabian Sea during 06–10 May 2002, the track errors after 24 and 48 h of integration with the quasi-Lagrangian model were 200 and 120 km, respectively; the track errors after 24, 36, and 48 h of integration with the Climatology and Persistence (CLIPER) model were 251, 329, and 533 km, respectively.

[31] The simulated tracks and intensities for TCs Kesiny and 01A are also shown in Figure 14 from the 10-day control run initialized at 0000 UTC 1 May. Despite the time difference in the formation of TCs Kesiny and 01A of about 89 h, which poses a challenge to predict both, the GMM predicts the genesis of TCs Kesiny and 01A at the right locations and times about 45 h (54 h) and 114 h in advance, respectively, successfully capturing the intensification process whereby initial weak storms/disturbances grow to become twin TCs. To our knowledge, no real-data simulation has ever been conducted to produce the genesis of twin TCs with realistic movement and intensification. The subsequent movement and intensity evolution of these twin TCs is also simulated reasonably well (e.g., Figures 14b and 14c), including Kesiny's re-curving on 3–5 May. Errors in the predicted location of Kesiny are 179, 283, 232, 115, 127, 95, 175, 438, 493 km after 48, 72, 96, 120, 144, 168, 192, 216, and 240 h of simulation, respectively. For TC 01A, the errors are 341, 97, 71, 114, 198 km after 120, 144, 168, 192, 216 h of simulation, respectively. Compared to the forecast position errors of TC 01A in the *WMO* [2004], the track forecast using a global model is very encouraging. While the initial intensity

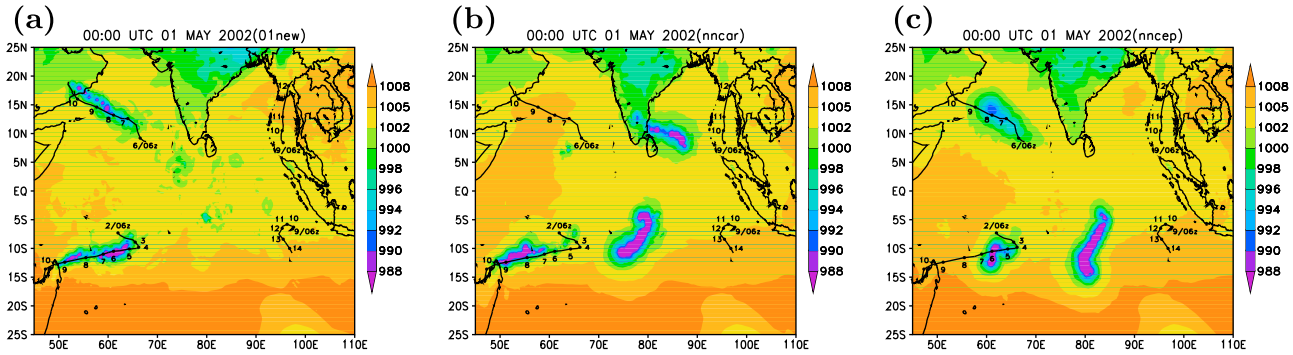

Figure 15. Minimum sea level pressure (MSLP) in the (a) CNTL, (b) EXP-A, and (c) EXP-B runs. The spatial distribution of MSLP over the 10-day integrations, which are initialized at 0000 UTC 1 May 2002, qualitatively shows the initial location and subsequent movement of the simulated TCs as well as over-intensified false positive storms. The ZM95 and H94 schemes are used in the EXP-A run, while the NCEP SAS scheme is used in the EXP-B run.

of Kesiny is overestimated as compared to the best track, presumably related to the initial vortex spin-up problem, its intensity is simulated quite well between 6 and 10 May after the formation of TC 01A. In comparison, the intensity of TC 01A is well predicted during its early lifecycle but is overestimated after 156 h of integration (Figure 14b), which is consistent with the excessive precipitation associated with disabling the CPs (not shown). It is worth mentioning that during 6–8 May, both the weakening of Kesiny and the intensification of TC 01A are realistically simulated.

[32] The implication from this global model simulation on the role of the large-scale environmental flow is as follows. As TC movement is largely steered by the large-scale flow, realistic simulations of the "subsequent" movement of TCs Kesiny and 01A after they formed suggest an important role for the "large-scale" flow in determining their movement. Due to the continuation of physical processes, one may expect that the "large-scale" flow may also play a role in determining the timing and location of their formation (before they formed). This indicates the advantage of using a global model, such as GMM, in improving the simulation of TC formation, movement and intensification; because it is required to know the global initial state if a forecast time span is greater than one week [*Smagorinsky*, 1967] Having discussed the modulation of TC formation by the large-scale waves in section 3.1, the feedback from small-scale moist processes (e.g., precipitation) are now examined to illustrate their impact on the simulations of developing and non-developing gyres.

3.3. Sensitivity of Simulations to Moist Processes and Initial Conditions

[33] It has been found that numerical simulations of hurricane formation are very sensitive to cases and also model physics [e.g., *Davis and Bosart*, 2002]. To address this, the three gyres, which are associated with one non-developing and two developing TCs, respectively, are simulated in two 10-day runs with different ICs, which are at 0000 UTC on 1 and 2 May 2002, respectively. In addition, different cumulus parameterization schemes are applied in the sensitivity experiments. In the following, the impact of using different moist processes on the simulation of the twin TCs' genesis are assessed in terms of their movement (Figures 15 and 17), associated precipitation (Figure 16) and the (horizontal) structures of the MRG wave (Figure 19).

[34] Figure 15 shows the spatial distribution of MSLP from three 10-day experiments to qualitatively display the initial location and subsequent movement of the simulated TCs. One of the major advantages with this kind of plot is the ability to check if a real TC or false-alarm event forms or appears in different locations during the period. Figures 15a, 15b, and 15c are results from the control (CNTL), EXP-A, and EXP-B runs, respectively. As discussed earlier, the CNTL run in Figure 15a simulates the formation and movement of the first twin TC realistically. In contrast, the EXP-A run fails to simulate the genesis of TC 01A (Figure 15b). Though the EXP-B run is able to simulate the formation of TC 01A, it simulates the TC 01A's genesis about 24 h later and also results in slower propagation speeds for both of the twin TCs than the best track (Figure 16c). In addition to the developing events, Gyre S_2 did not develop in the control run but did intensify and lead into false-alarm events in both the EXP-A and EXP-B runs. These experiments suggest that TC simulations significantly depend on the parameterizations of moist processes. The simulated precipitation associated with these three events is examined below.

[35] In section 3.3, it was shown that the formation of twin TCs can be predicted up to 5 days in advance with a time lag of 3 days between the formation of the first and second TCs. During the period 1 to 6 May, these three gyres went through different stages of their lifecycles, including the initial formation of TC 01A, the intensification of Kesiny, and the intensification and then weakening of the false-alarm event. Therefore, to simplify the discussions, only the spatial distributions of "averaged" precipitation from 3 to 6 May will be analyzed to illustrate the overall performance (or general difficulties) of a specific scheme in simulating the aggregate effects of precipitation processes at regional scales associated with these events at their different stages. An average is used simply because precipitation fluctuates at timescales shorter than the large-scale circulation. In addition, the relatively coarse resolution and the stochastic nature of the individual convective cells make it very challenging to reproduce the small spatial and temporal variability of precipitation. It

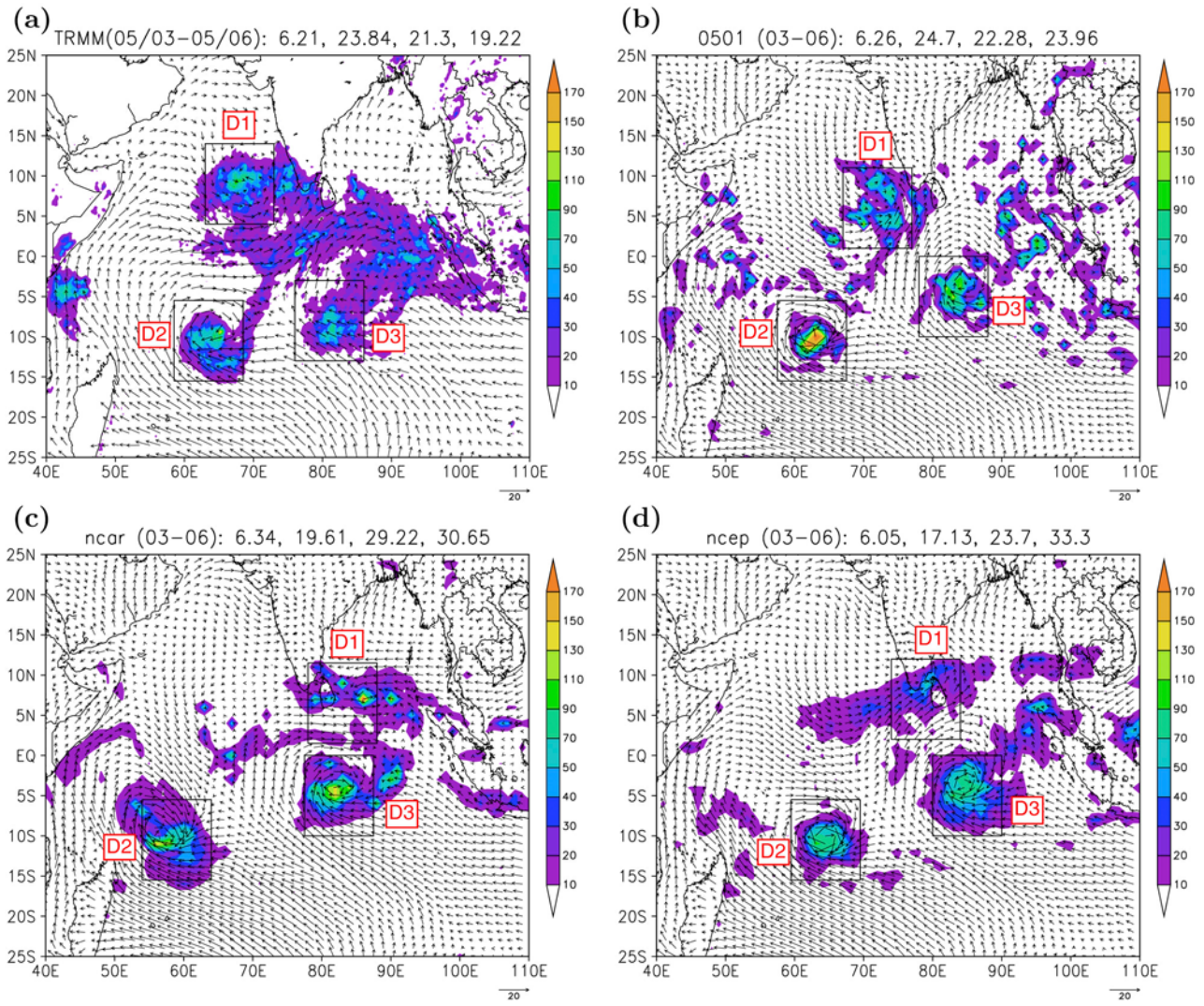

Figure 16. Precipitation (mm/day) and surface winds averaged over 3–6 May 2002 from (a) NASA TRMM (shaded) and QuikSCAT winds (vectors), (b) the CNTL run, (c) the EXP-A run and (d) the EXP-B run. Each of the three black boxes contains a local precipitation maximum and is used to calculate domain-average precipitation from the corresponding numerical experiments. Figures 16b–16d show 10 m winds from the simulations initialized at 0000 UTC May 1.

should be noted that quantitative precipitation forecasts on a time scale of 5 days is still challenging at operational NWP centers. As follows, simulated surface winds and precipitation are compared with NASA QuikSCAT winds and TRMM precipitation to discuss: (1) the performance of moist processes in simulating precipitation at regional scales in association with the three events, (2) the dependence of simulated TC formation on the different moist schemes, and (3) the impact of different moist processes on the appearance of the false-positive event associated with the non-developing event.

[36] Figures 16a–16d show precipitation (shaded) and surface winds (vectors) averaged over 3–6 May 2002 using data from NASA satellites (e.g., TRMM precipitation and QuikSCAT winds) and the CNTL, EXP-A, and EXP-B runs, respectively. The CNTL run simulates realistic amounts and spatial distributions of precipitation for the three events. In contrast, the parameterized moist processes associated with a specific CP and their nonlinear interactions with other physical processes led to the under-development of Gyre N_1 but the over-development of Gyre S_1. For quantitative comparison, precipitation over the large domain (25°S–25°N; 40°E–110°E, see Figure 16) and three additional 10° × 10° sub-domains is further averaged to understand the model's performance in simulating precipitation at regional scales. Each of these sub-domains (labeled D_1-D_3) is selected to be close to one of the three major convective events (associated with the three gyres) and is centered on a precipitation maximum. Note that D_1 in the two parallel runs (e.g., EXP-A and EXP-B runs) is not realistic, because TC 01A did not appear in these runs. These domain-averaged precipitation amounts from TRMM and all of the experiments are summarized in Table 2. It is clear that the control run with its explicit moist scheme produces the best results over the large domain and the three sub-domains.

Table 2. Spatial and Temporal Averaged Precipitation (mm/d) During the Period 0000 UTC 3 to 0000 UTC 6 May 2002 From TRMM and Numerical Simulations, Including the Control, EXP-A, EXP-B and EXP-E Runs[a]

	TRMM	CNTL	EXP-A	EXP-B	EXP-E
D_L	(0°, 75°)	(0°, 75°)	(0°, 75°)	(0°, 75°)	(0°, 75°)
D1	(9°, 68°)	(6°, 72°)	(6.5°, 83°)	(7°, 79°)	(6°, 70°)
D2	(−10.5°, 63.5°)	(−10.5°, 62.5°)	(−10.5°, 59°)	(−10.5°, 64.5°)	(−11°, 63.6°)
D3	(−8°, 81°)	(−5°, 83°)	(−5°, 82.5°)	(−5°, 85°)	(−5°, 83°)*
P_L (mm/d)	6.21	6.26	6.34	6.05	6.33
P1 (mm/d)	23.84	24.7	19.61	17.13	28.87
P2 (mm/d)	21.3	22.28	29.22	23.7	27.2
P3 (mm/d)	19.22	23.96	30.65	33.3	17.05
E_L (%)	na	0.81	2.1	−2.58	1.9
E_1 (%)	na	2.35	−17.7	−28.15	21
E_2 (%)	na	4.6	37.2	11.27	27.7
E_3 (%)	na	24.67	59.5	73.26	−11.3

[a]The large domain (D_L) covers the area (25°S–25°N, 40°E–110°E). Three additional 10° × 10° sub-domains (D_1, D_2, D_3) are centered on the precipitation maxima associated with TCs 01A, Kesiny, and the organized (non-developing) convective event, respectively. These domains are shown by the black boxes in Figure 16. **D_i,** i = L, 1, 2, 3* indicates the (lat, lon) of the corresponding domain center. **P_i** (mm/d) indicates the domain average precipitation, while **E_i** is the relative error in the domain-averaged precipitation. **E_i** = $(P_i\text{-}P_{TRMM})/P_{TRMM}$, where P_{TRMM} is the corresponding domain average precipitation from TRMM. D_3 in EXP-E is the same as that in the control run.

[37] As shown in Figures 15b and 15c, both the EXP-A and EXP-B runs underdevelop Gyre N_1 and overdevelop Gyre S_2. In Figures 16c and 16d, the simulated precipitation amounts are consistent with those results with precipitation underestimated for Gyre N_1 and overestimated for Gyre S_2. Previous studies [e.g., *Vitart et al.*, 2001] suggested that CPs may stabilize the environmental flow and limit TC formation, which is supported by the simulation of TC 01A in both EXP-A and EXP-B. However, these two runs also unrealistically intensified Gyre S_2 such that it became a false-alarm event. Comparing runs CNTL, EXP-A and EXP-B suggests that CPs, which were implemented with the assumption of quasi-equilibrium and a universal time scale (e.g., the relaxation time), may be valid at a TC's mature stage but not during the formation stage, which is consistent with the discussions in *Ooyama* [1982]. Specifically, although the parameterization of CP was an important technical factor in the reduction of a multiscale interaction problem to a mathematically tractable form [*Ooyama*, 1982], it is now known that the validity of CPs at a resolution of 10–40 km becomes questionable. With these resolutions, the deep cumulus becomes resolvable, so it is difficult to separate physical processes with the grid-scale and sub-grid scale, which is required by the quasi-equilibrium assumption, and thus the impact of latent release may be double counted when the large-scale condensation scheme is also applied [*Molinari and Dudek*, 1992] In addition, these results also imply that the performance of a specific CP scheme varies under different "large-scale" conditions (e.g., different gyres), suggesting a dependence on ICs. Though the CNTL run with explicitly grid-resolved moist processes produced the best results, this approach does simulate some grid point storms, which should be carefully addressed in a future study.

[38] To illustrate the impact of regional change in the moist processes, the spatial distributions of MSLP from the EXP-C and EXP-D runs are shown in Figure 17. These two runs disable the CPs in a global channel from 0° to 40°E and 40°S to 0°, respectively, and apply ZF96 and H94

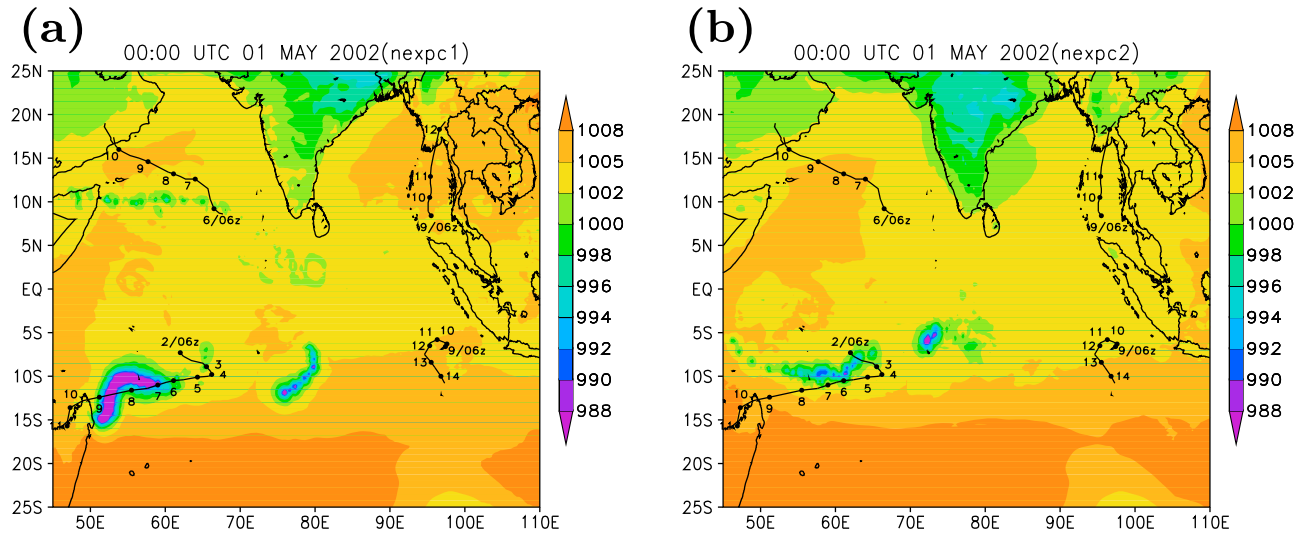

Figure 17. Same as Figure 15 except for the (a) EXP-C and (b) EXP-D runs. These two runs disable CPs in a global channel (i.e., from the equator to 40°N in EXP-C and from 40°S to the equator in the EXP-D) and enable the ZM95 and H94 schemes elsewhere.

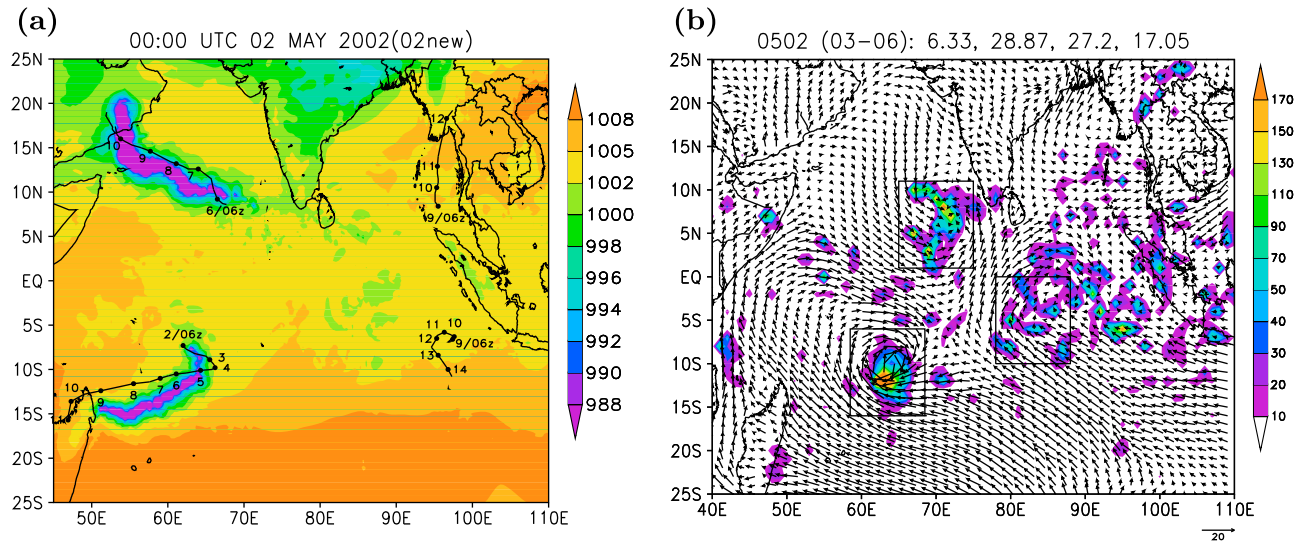

Figure 18. Same as (a) Figure 15 and (b) Figure 16 except for the EXP-E run with a different set of ICs (i.e., 0000 UTC 2 May 2002). Each of the three boxes in Figure 18b is used to calculate domain-average precipitation.

everywhere else. The EXP-C run was designed mainly to understand if the simulation of TC 01A's formation could be improved with respect to the EXP-A run, while EXP-D was made to examine the simulation of Gyre S_2. It is shown that simulations of TC 01A in EXP-C and Gyre S_2 in both EXP-C and EXP-D are improved slightly as compared to EXP-A. However, these results also suggest that regional changes in the moist processes may not be sufficient to improve the *accuracy in the* simulation of TC 01A's formation (e.g., EXP-C) or the evolution of Gyre S_2 (e.g., EXP-D) because they may involve interactions with the large-scale environmental flow, such as the MRG wave. Brief discussions on the association of these gyres with the MRG wave are given below in Figures 19 and 20.

[39] The last experiment, EXP-E, was made to show the sensitivity of the simulations to a different set of ICs (i.e., 0000 UTC 2 May 2002). The spatial distribution of the MSLP during the 10-day period suggests that the formation of the twin TCs is captured realistically and their subsequent movement is also simulated with some degree of satisfaction (Figure 18a). The simulation is slightly less accurate than the CNTL run but more realistic than the EXP-A and EXP-B runs with CPs. Precipitation (mm/day) averaged over 3–6 May 2002 is shown in Figure 18b, which can be compared with TRMM and the control run in Figure 16. Domain-average precipitation inside each of the three boxes is listed in Table 2. Overall, the spatial distribution of the precipitation associated with the three gyres is comparable to that in the CNTL run (e.g., the location of each sub-domain listed in Table 2). However, the domain-averaged precipitation has larger errors than the CNTL run, which suggests there may be a dependence on ICs or with the model spin up. It is, however, encouraging that the average precipitation in the large domain and three sub-domains in EXP-E is better than in EXP-A and EXP-B as shown by the corresponding relative errors in Table 2 (note that the D_1 domain selected in both EXP-A and EXP-B is not associated with a realistic Gyre N_1 or TC 01A).

[40] Sensitivities of the MRG wave and TC simulations to different settings in the moist processes and a different set of ICs are shown in Figure 19. Figures 19a–19h show the meridional winds (shaded) and geopotential heights (contours) at 0000 UTC 6 May 2002 from NCEP T254 analyses, NCEP 2.5° reanalyses, and the CNTL, EXP-B, EXP-A, EXP-C, EXP-D, EXP-E runs, respectively. To facilitate discussions on the genesis of TC 01A, a vertical line is plotted at longitude 70°E. Comparing the panels suggests: (1) the northerly winds along 90°E are better represented in the NCEP 2.5° reanalyses than in the T254 analyses, which therefore suggests that the CNRL run realistically simulated the intensification of the MRG wave at this time (e.g., Figure 19c and Figure 8f), (2) the nongenesis (or inaccurate genesis) of TC 01A in the EXP-A (EXP-B) run is associated with a faster (slower) westward propagation speed of the MRG wave, (3) among the EXP-A, EXP-C and EXP-D runs where ZF95 and H94 are applied globally or in a global channel, little differences appear in the simulation of TC Kesiny, but significant differences appear in the simulation of TC 01A and the associated MRG wave, and (4) the EXP-E run (Figure 19h) initialized at 0000 UTC 2 May 2002 produces the simulations of the twin TCs and the MRG wave that are comparable to the control run (Figure 19c). A more detailed evaluation on the phase and amplitude of the simulated MRG wave and their impact on TC genesis is being conducted.

[41] It has been shown that the wave number of a mode can be modified by background longitudinal stretching deformation, namely dU/dx, U is the background wind speed. When the background flow contains negative stretching deformation, the wave's scale decreases and its amplitude increases. This is the so-called wave accumulation processes, which was first proposed by *Webster and Chang* [1988]. In recent years, it has been applied to explain the intensification of an ER wave that could lead the formation of a TC [e.g., *Molinari et al.*, 2007]. The relation between a deepening and shortening MRG wave and its association with

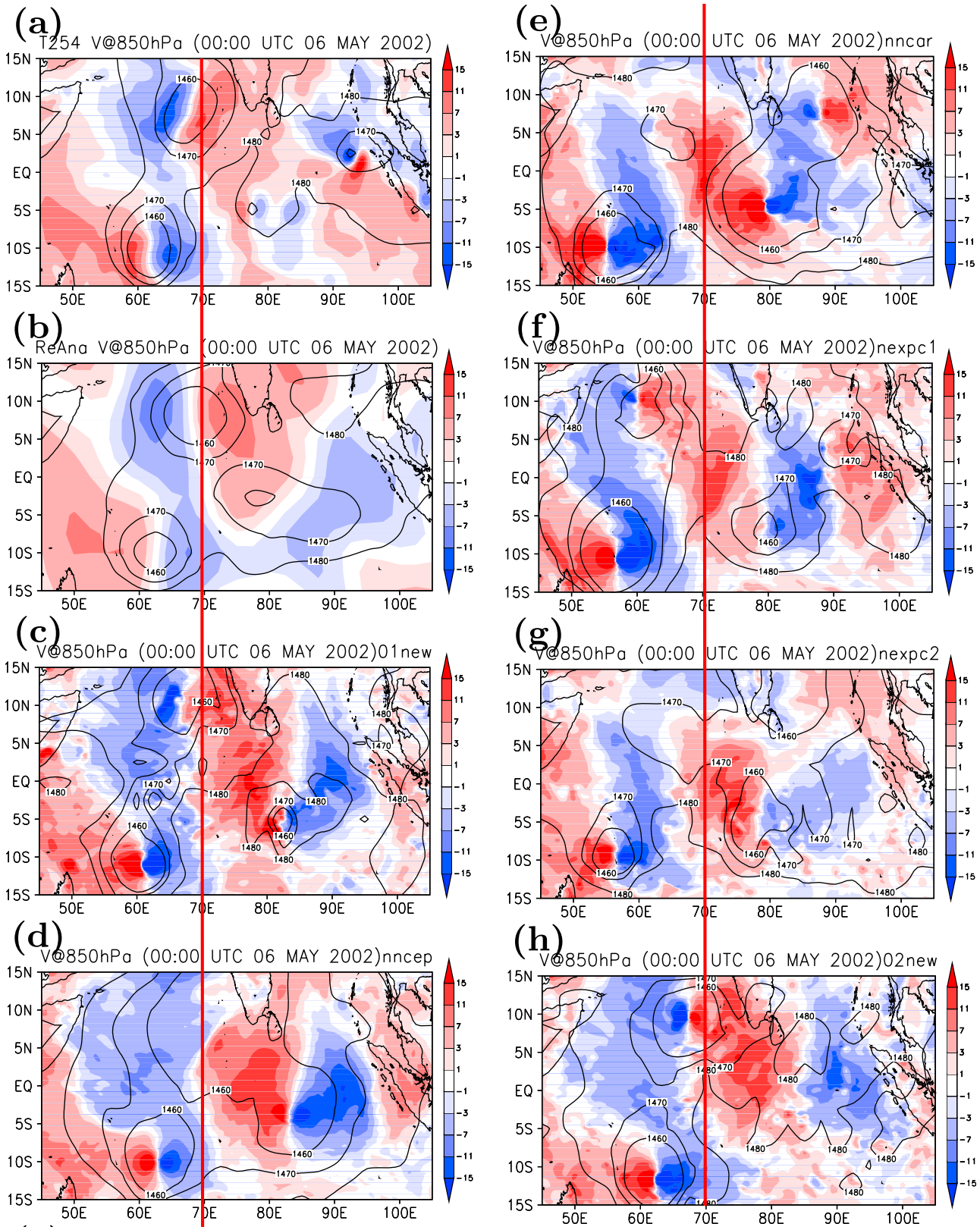

Figure 19. The 850-hPa meridional winds (shared) and geopotential heights (contours) at 0000 UTC 6 May 2002 for (a) NCEP T254 analyses, (b) NCEP 2.5° reanalyses, (c) the CNTL run, (d) EXP-B, (e) EXP-A, (f) EXP-C, (g) EXP-D, and (h) EXP-E. Selected contour lines of geopotential heights include 1460, 1470 and 1480 m. Note that EXP-E is initialized by a different set of ICs and is still compared well with the CNTL run.

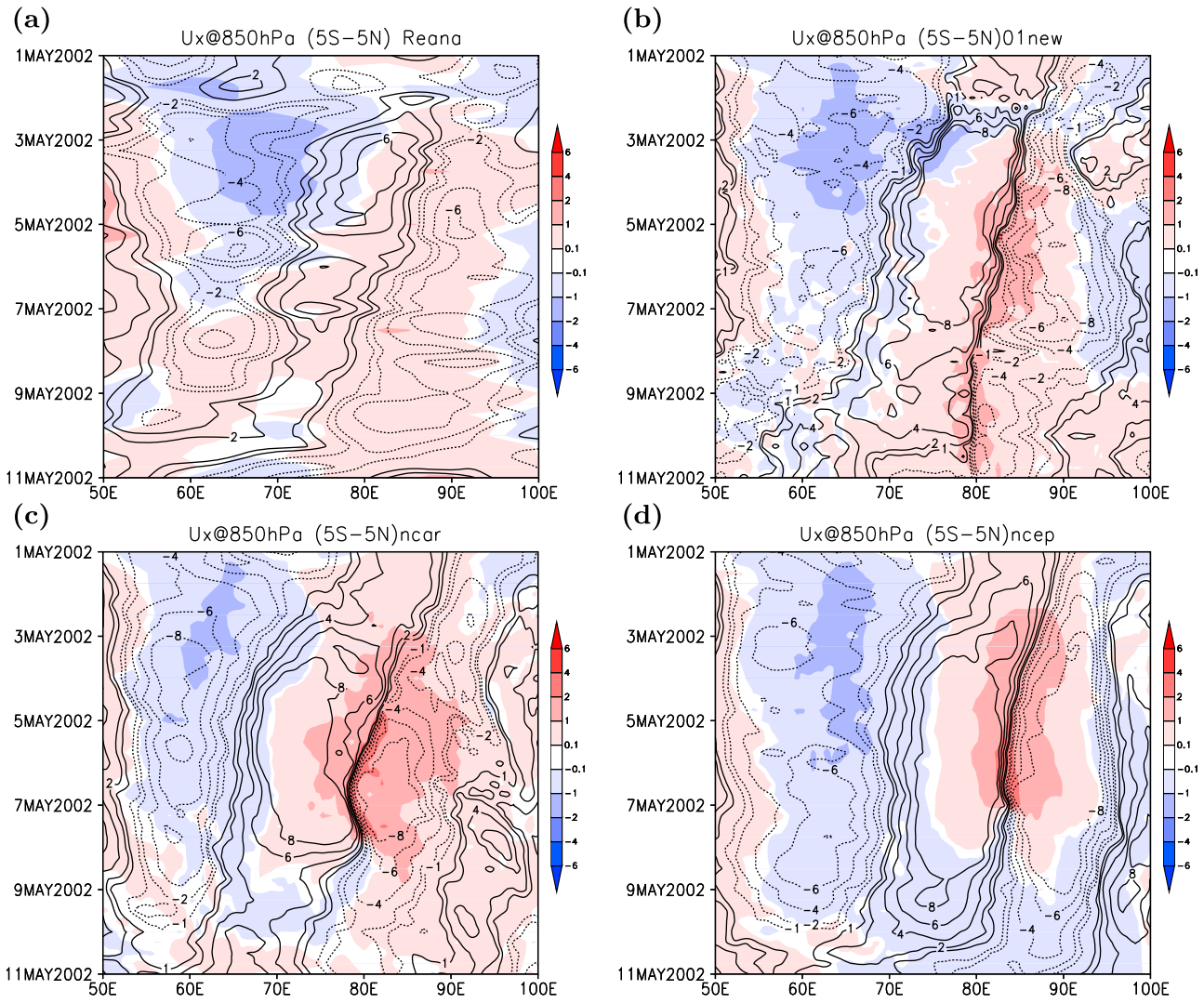

Figure 20. Hovmoller diagram of the longitudinal stretching deformation ($10^{-5}s^{-1}$, shaded) and meridional winds (contours) averaged over latitudes 5°S and 5°N. (a) NCEP Reanalysis, (b) the CNTL run, (c) the EXP-A run, and (d) the EXP-B run.

stretching deformation is discussed below. To avoid the complication in decomposing the total zonal winds into the background mean winds and wave perturbations which involve complicated mean-wave and wave-wave interactions, we choose to calculate the stretching deformation of the total zonal winds. Since we are interested in the impact of stretching deformation on wave shortening and deepening, which may help predict the timing of TC formation, a Hovmoller diagram of the stretching deformation ($10^{-5}s^{-1}$) is plotted in Figure 20. While Figure 20a shows the NCEP reanalysis data (at a resolution of 2.5°), Figures 20b, 20c, and 20d show the results from the CNTL, EXP-A and EXP-B runs. Negative stretching deformation (blue), which indicates wave accumulation, appeared in the areas between 60°E and 80°E from May 1 to 5, 2002. The appearance of the local minimum (with the magnitude greater than 1×10^{-5} s^{-1}) between longitudes 65°E and 72°E from May 3 to 5 is consistent with the intensification of the MRG wave (e.g., solid contour lines in Figure 20a; also shown in Figure 5a). Overall, a comparison of the CNTL run and these two experiments with the NCEP reanalysis suggests that the control run produces the best evolution of the stretching deformation (e.g., blue areas) in terms of timing and location. This is important for improving the prediction of TC 01A formation. Note that the control run and the other experiments as well is able to reveal the evolution of shear deformation at smaller scale near gyres N_1 and S_1 than the reanalysis.

[42] Figure 21 shows a Hovmoller diagram of the vorticity ($10^{-5}s^{-1}$) from the CNTL, EXP-A, EXP-B, and the EXP-C runs. Neither NCEP reanalysis nor analyses data are used in this plot, because the former has coarse resolution that cannot accurately resolve the mesoscale vortex and thus vorticity and the latter are available only at a time interval of one day. Vorticity is defined here as (dv/dx – du/dy). Positive values correspond to cyclonic (anti-cyclonic) circulations in the NH (SH). Shaded areas show vorticity averaged over latitudes 10°S and 0°, while contour lines show vorticity averaged over latitudes 0° and 10°N. Note that only positive contour lines are plotted and thus dense contour lines indicate the

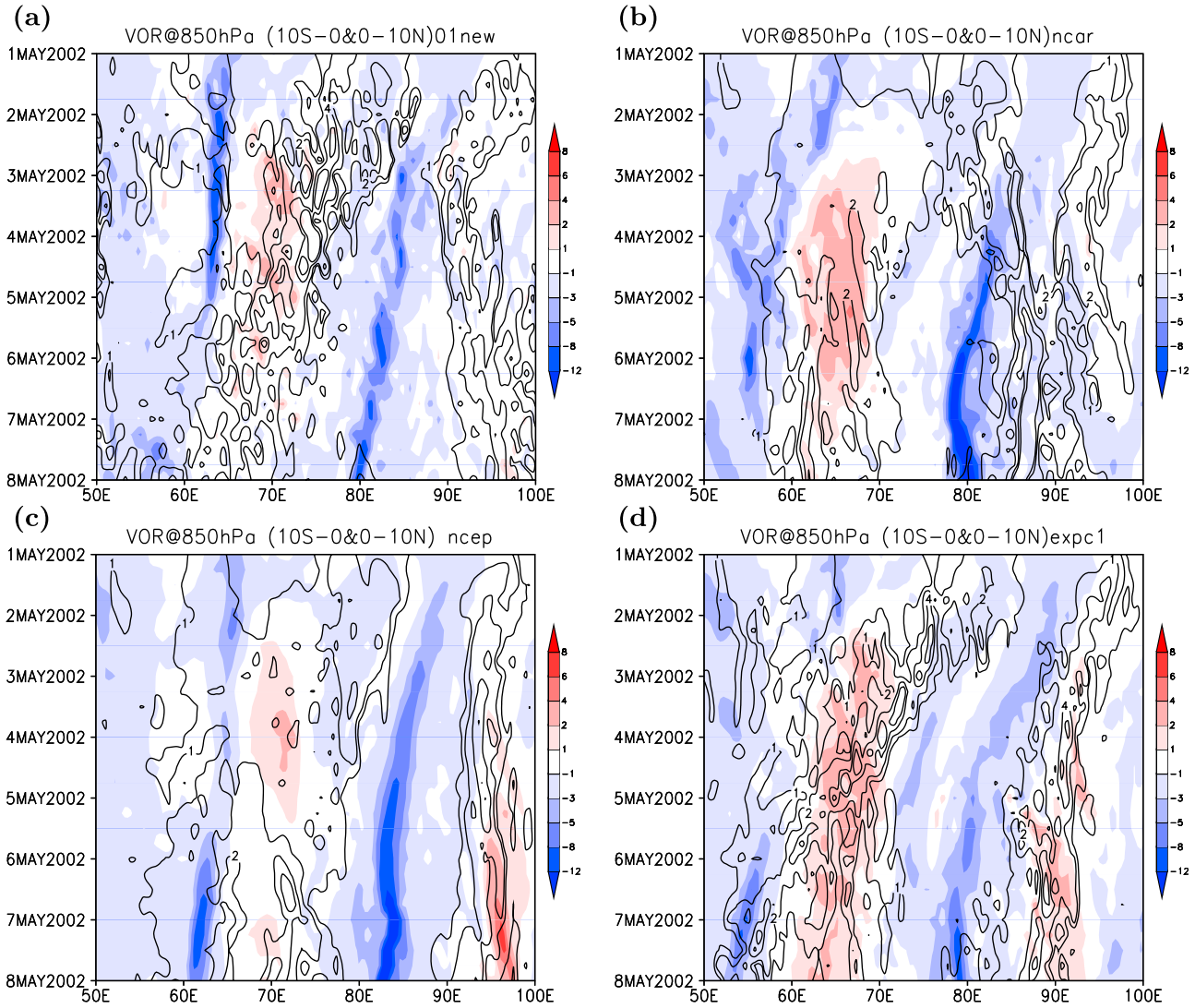

Figure 21. Hovmoller diagram of the vorticity ($10^{-5}s^{-1}$). Shaded areas show vorticities averaged over latitudes 10°S and 0°, while contour lines (with selected values of 1, 2, 4, and 6 × $10^{-5}s^{-1}$) show vorticities averaged over latitudes 0° and 10°N. (a) The CNTL run, (b) the EXP-A run, (c) the EXP-B run, and (d) the EXP-C run. Local minima (blue) indicate the locations of gyre S_1 and gyre S_2. Dense contour lines between gyres S1 and S2 indicate the location of gyre N_1.

location of gyre N_1. Thus, local minima (blue) indicate the locations of Gyre S_1 and Gyre S_2. Between these two gyres, positive vorticity in the NH (shown by the contour lines) indicates the gyre N_1. During the period of May 1–4, gyres S_1 and S_2 approach each other, indicating a wavelength reduction (Figure 21a). During this period of wavelength reduction, the red areas between gyres S_1 and S_2 indicate the southern portion of the circulation associated with the gyre N_1. Note that as TC 23S and TC 01A moved southwestward and northwestward, respectively, they moved outside the latitudes of 10°S and 10°N at later times, thus no visible in Figure 21a. In comparison, the simulated strength of gyre S_2 is overestimated after 4∼5 May 2002, which was shown in the averaged precipitation in Figure 16. The EXP-A run did not capture the evolution of wave shortening and the formation of TC 01A well (Figure 21b). Compared to the CNTL run, the EXP-B run (Figure 21c) simulates a comparable evolution of the wave shortening but weaker vorticities during the first three days. Thus, no TC (i.e., TC 01A) appeared at the right time in the NH. Interestingly, as the EXP-B run simulates TC 23S at much slower speeds (Figure 15c) and gyre S_2 with a stronger intensity during the period of May 4∼5, a model TC appeared at a later time (24 h later than the best track) in the NH, shown by the contour lines in Figure 21c. This may also indicate the importance of the appearance of the MRG wave in "determining" the location and timing of TC 01A's genesis, though wave shortening is not very clear in this case. The latter might indicate the importance of improved moist processes at a regional scale (e.g., near gyre N_1) in the simulation of TC 01A genesis. We illustrate this with a simple comparison between the EXP-A and EXP-C runs. While both runs with less accurate simulated evolutions of the MRG's wavelength (as compared to the CNTL run) (Figures 21b and 21d), the

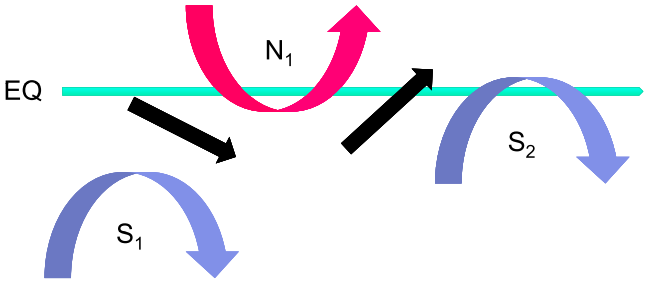

Figure 22. Conceptual diagram of the scale interactions between the three gyres. Both S_1 and S_2 are in the SH, and N_1 is in the NH. Black arrows indicate winds, which can be a measure of the MRG wave strength. Therefore, the MRG wave can intensify in association with either a reduction in the wavelength (the distance between S_1 and S_2) and/or the intensification of individual gyres.

EXP-C run with disabled CPs between latitudes 0 and 40°N was still able to simulate the formation of TC 01A. However, the EXP-C run has larger errors in the location and timing of TC 01A formation and its predicted movement and intensification (Figure 17a) is less accurate than the control run (Figure 15a).

[43] Figure 22 is conceptual model summarizing the importance of the accurate simulations of wave deepening or intensification of the MRG wave (near the equator, shown in Figure 4 and Figures 8f and 8j) in the formation of TC 01A. The wave deepening appears to be associated with (1) the process of wave shortening or (2) the intensification of individual gyres (e.g., N_1 or S_1) if the wavelength remains unchanged. The first process is revealed by a reduced distance between gyres S_1 and S_2 in Figures 5 and 6 and negative longitudinal stretching deformation in Figure 20, and indicates the importance of accurate representation in the evolution of the large-scale wave that is influenced by the environmental flows (e.g., negative longitudinal stretching deformation). The second process indicates that the horizontal phasing of the southwesterly winds of gyres N_1 and S_1 may lead to wave deepening if one of them is intensified (or moving closer), which can be shown by the improved simulation of gyre N_1 in the EXP-C run as compared to the EXP-A run (Figures 21b and 21d) and or the falsely intensified gyre S_2 in the EXP-B run (Figures 21a and 21b). Therefore, the second one suggests the importance of accurate representations of the vortex circulation and thus aggregate feedbacks of precipitation processes at the mesoscale. Note that nonlinear interactions might exist between the first and the second processes. For example, as the wave deepening occurs in association with wavelength reduction and negative stretching deformation from May 2–5 (Figure 20), convection tends to become active and contribute to the intensification of the gyres, which can be shown in Figure 16 with heavy precipitation near the gyres.

4. Concluding Remarks

[44] In this study, numerical simulations from a global mesoscale model are presented to address the formation of twin TCs (Kesiny and 01A) that occurred during an active phase of the MJO in the Indian Ocean in early May 2002. This is one of a series of modeling studies [e.g., *Shen et al.*, 2010a, 2010b] that aim to understand the role of tropical waves in the formation of TCs and the predictive relationship between them with the goal of extending the lead time for predicting TC genesis. Previously, the association of an equatorial Rossby wave and an AEW with the formation of TC Nargis (2008) and Hurricane Helene (2006) was studied in *Shen et al.* [2010a] and *Shen et al.* [2010b], respectively. In this study, the role of a ccMRG wave disturbance, which appeared as an integral of three gyres and intensified in the convectively active envelope of the MJO, in the formation of twin TCs is examined. Based on the analysis of NCEP reanalysis, the MRG wave has an averaged wavelength of about 30°, a period of about 7 days, and a westward phase speed of (−1.8 m/s). These features are close to the theoretical values from the dispersion relation of a linear MRG wave with an equivalent depth of 90 m and an averaged background zonal wind speed of 3.71 m/s. Six 10-day 0.25° simulations are discussed, five of which were initialized at 0000 UTC 1 May and one at 0000 UTC 2 May. The control run predicted the genesis of TCs Kesiny and 01A realistically about 2 and 5 days in advance, respectively, as well as their subsequent movement up to 10 days. The other five experiments were conducted to examine the sensitivities of the numerical simulations to the moist processes with different CPs as well as a different set of ICs. Results from these experiments suggest that the predictability may be attributed to the improved simulation of the ccMRG wave and the associated small-scale moist processes. Major processes that are crucial for the formation of the twin TCs are summarized as follows:

[45] 1. Deepening of the ccMRG wave in association with wavelength reduction or the intensification of individual gyres (e.g., S_2). Initially, a westward-moving MRG wave with baroclinicity appeared as the integral of three gyres (S_1, N_1 and S_2); scale reduction was indicated by the faster westward phase speed of gyre S_2 than that of gyre S_1. The wavelength reduction is consistent with the appearance of negative stretching deformation of the zonal winds.

[46] 2. Poleward movement (or cut-off) of a gyre (e.g., N_1) that may be influenced by boundary layer processes. There existed a westward phase lag of 1/4 wavelength between the vertical pressure velocity maximum and the low level (e.g., 850 hPa) southerly wind maximum, which resembles a TD-type disturbance. However, the phase relationship at middle levels (e.g., 500 hPa) is still similar to that of a free MRG wave. Therefore, the MRG wave has a hybrid structure of the MRG-type and TD-type disturbances. As suggested by *Holton* [1975], boundary layer processes are responsible for this phase lag and may lead to the cut-off of the gyre.

[47] 3. Realistic spatial distributions of precipitation associated with the initial intensification of the three gyres during May 3–6 (Figure 16), which is consistent with the simulated locations of the Gyres S_1 and N_1 and also consistent with the simulations of vertical pressure velocities in Figure 13. The simulations support the finding of *Aiyyer and Molinari* [2003] that the poleward movement is related to the diabatic heating.

[48] 4. Development of low- and mid-level CCs near Gyre N_1. As time progresses, the low- and mid-level CCs associated with Gyre N_1 moved westward and northward and became "coherent" vertically, providing a favorable condition for TC genesis with the zero vertical wind shear

line centered on the CC. Simulations of this vertical coherence in the CCs at different levels (e.g., on May 5 and 6 in Figure 12) are consistent with the simulations of precipitation (in Figure 16), which are associated with deep convective processes.

[49] Even though the simulations of average precipitation are consistent with the simulations of Gyres S_1 and N_1, the causality between these gyres (and the ccMRG wave) and the diabatic heating remains unclear and is subject to a future study. Specifically, due to the nonlinear interactions between the heating and the MRG wave, the current study is not yet sufficient to conclude that the adiabatic heating acts as a forcing to drive the evolution of the MRG wave. After TC Kesiny and 01A formed on May 3 and 6 respectively, these two TCs moved at different speeds and gradually evolved into twin TCs. In addition, the gyre S_2, which resembles an MRG wave well, started weakening after May 6 (e.g., Figure 2a). All of these "appear" as a transition of an MRG wave into an equatorial Rossby wave. In contrast, the scale interactions of the three gyres can be conceptually viewed as the interactions between an ER (consisting of gyres S_1 and N_1) and a MRG wave mode (gyre S_2, e.g., Figure 21). All of these are subject to further examination.

[50] Although the MRG wave provides an integral view on the activity of the three gyres, accurate simulations of the MRG wave require realistic simulations of each of the three gyres. Moreover, it is important to realistically capture the spatial distributions of precipitation associated with the three different gyres that may move at different speeds. The results indicate the difficulty of simulating these phenomena using a model with CPs, presumably because CPs are column based and are less sensitive to adjacent grid columns. Parallel experiments with CPs enabled in the global environment or a global channel suggested that the performance of the associated moist processes in the specific settings depended on the ICs, namely the performance differs for different gyres. For example, in both EXP-A and EXP-B, gyre N_1 was underestimated while gyre S_1 was overestimated. Therefore, a future study is needed to examine if the model with different moist schemes or different ICs may experience different spin-up processes, leading to an improper tendency in the intensity evolution of the gyres, which may require further model calibrations or tuning. In contrast, the control run with an explicit large-scale condensation scheme produced the best predictions for the two developing and one non-developing event(s). The EXP-E run with the same setting as those in the control run but with different ICs also generated better results than the other experiments with CPs. A similar conclusion that better results appeared in the runs with no CPs was also made in *Shen et al.* [2010a, 2010b]. However, these limited case studies are still not sufficient to conclude that 1/4 degree simulations do not need CPs. Instead, the importance of understanding the performance of a specific CP (or other column-based physics parameterization) in simulating multiple organized convective events and their spatial distribution with regards to representing the large-scale flow (e.g., a ccMRG wave) is emphasized.

[51] It should be emphasized that in treating the numerical model as a tool, we would prefer to focus first on the TC genesis that is predictable, so that we may gain confidence in the model's ability to simulate hurricane climate. Based on the current study and two previous studies [*Shen et al.*, 2010a; 2010b] using the global mesoscale model, the following view on the predictability of mesoscale TC genesis is proposed: (1) Both a downscaling cascade of processes associated with the large-scale systems and an upscaling cascade of processes associated with the small-scale (e.g., precipitation) systems are important. Because of the asymmetry in the spatial and temporal scales and the strengths among these systems, the term "hierarchical multiscale interactions" is used to describe these scale interactions that can lead to TC formation. (2) Large-scale tropical waves such as an MRG wave may provide determinism in regards to the timing and location of TC genesis, which can be viewed as a pre-cursor. (3) Since a larger-scale system (i.e., the precursor) has better predictability, it becomes possible to extend the lead time for TC genesis prediction as long as the model can improve the simulations of the precursor and its modulation on TC activities. (4) Accurate simulations of convective-scale processes remain challenging, but their aggregate feedbacks to TC genesis, especially under strong "forcing" such as with an MRG wave or an equatorial Rossby wave, can be simulated with some degree of satisfaction (e.g., this study and *Shen et al.* [2010a]). Further studies should focus on how these small-scale processes with a short life cycle can efficiently feedback to a TC (or gyre) or MRG. For example, the next stage will be verifying the so-called Marsupial Paradigm [*Dunkerton et al.*, 2008] hypothesis that a large-scale tropical easterly wave with a critical layer/level (CL) may provide a small "protected area" within which small-scale processes can develop and efficiently provide upscale feedback that leads to TC genesis.

[52] Based on the aforementioned discussions, further improvement to the realistic evolution of MRGs using the global mesoscale model could enhance the ability to predict TC genesis. As the occurrence of an MRG wave may be associated with the large-scale MJO, it becomes important to improve the simulation of the MJO (e.g., its eastward movement) to extend the lead time of the MRG wave simulations, especially their eastward moving component. Further studies should focus on the role of moist processes in the simulation of the MJO and MRG waves, because their evolution (in particular their poleward propagation/movement [e.g., *Aiyyer and Molinari*, 2003]) is dependent on the diabatic heating associated with the large-scale organized moving convective processes. As the MJO in May continuously moved eastward, a second pair of twin TCs appeared on May 9 in the Indian Ocean, and two additional TCs, super-typhoon Hagibis and Hurricane Alma, formed in mid-May in the West and East Pacific. Three additional 10-day numerical experiments initialized at 0000 UTC on 6, 11, and 22 May have been performed to simulate the formation of these four TCs. Preliminary analyses suggest that an equatorial Rossby wave may be the precursor to the formation of the second twin TCs, and an MRG-type or TD-type disturbance might be associated with the formation of super-typhoon Hagibis in the West Pacific, but no wave-like (no ER, MRG wave or TD-type disturbance) signal appears to be associated with Hurricane Alma in the East Pacific. This leads to the question of how and when an MRG wave could be excited in association with the MJO. A further study examining the excitation of MRG waves is being conducted

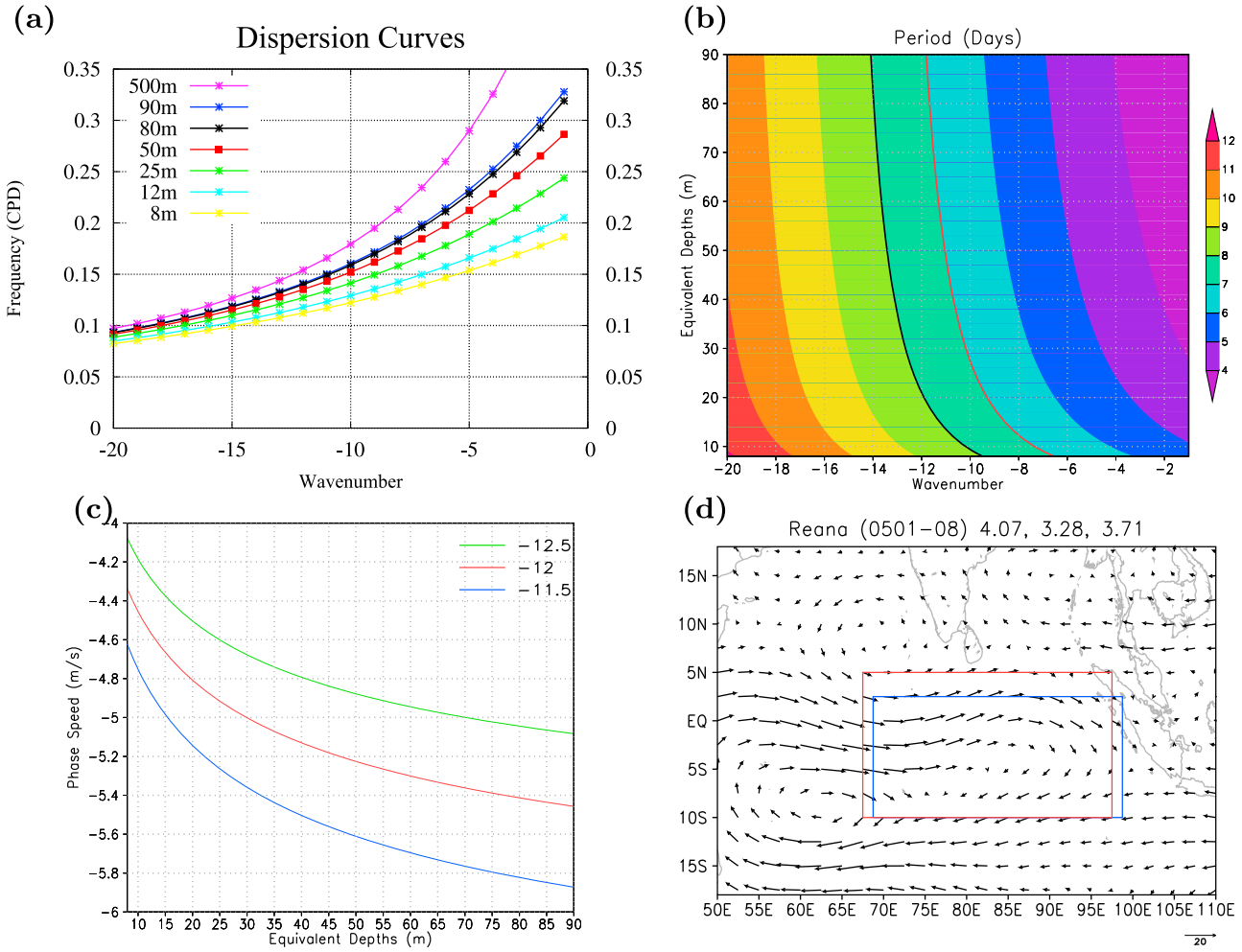

Figure A1. Dispersion relation as a function of frequency (ω), wave number (k) and equivalent depth (H). (a) Dispersion curves in the k- ω space with equivalent depths (H) of 8, 12, 25, 50, 80, 90, and 500 m in different colors. (b) Wave periods (days) in the k-H space. The red (black) line indicates the period of 7 (8) days. (c) Phase speeds (m/s) at function of H for k = −11.5 (green), k = −12 (red), and k = −12.5 (blue). (d) NCEP 850-hPa wind speeds averaged over a 7-day period between 0000 UTC May 1 and 0000 May 8, 2002. Zonal speeds averaged over the red box and the blue box are 4.07 m/s and 3.28 m/s, respectively. The domain-weighted averaged value of these two is 3.71 m/s.

with this case and additional MJO cases in support of the Year of Tropical Convection (YOTC) project. The next step is to examine if and how a global mesoscale model can improve extended-range (∼30 day) simulations of the MJO, its association with MRG waves and TC genesis in different basins.

Appendix A: Dispersion Relation of the MRG Wave

[53] In this appendix, we discussed how the wavelength and phase speed of the MRG wave are estimated and whether they are consistent with the linear dispersion of the dry MRG wave. Note that as active convection (of the MJO) was associated with the MRG wave, it is not realistic to expect an exact match between the observed and theoretical phase speeds [e.g., *Dickinson and Molinari*, 2002]. In addition, as the MJO moved eastward, suggesting the potential existence of other disturbance with an eastward group speed, we did not make an attempt at determining the group speed of the MRG wave from either the reanalysis or model simulations. From Figure 5a, the wavelength is about 30° (e.g., the distance between the two minima on 4 May 2002.), which gives the wave number of 12. The corresponding phase speed is roughly equal to the reciprocal of the slope of a constant phase line. The black arrow near the label S2 in Figure 5a indicates a distance of 10° during a 7 day period, which gives an estimated phase speed of −1.8 m/s. Next, we compare these estimated values with those from the linear shallow water solution [e.g., *Matsuno*, 1966].

[54] Figure A1a shows the dispersion curves with the following dispersion relation:

$$\omega = \frac{k\sqrt{gH}}{2}\left[1 - \left(1 + \frac{4\beta}{k^2\sqrt{gH}}\right)^{1/2}\right].$$

[55] Here, ω and k are the frequency and wave number, respectively; g is the acceleration of gravity; H is the

equivalent depth. β, which is the variation of the Coriolis parameter with latitude, is the so-called Rossby parameter. When the basic state zonal flow has a constant wind speed of U, the above dispersion is modified by a Doppler effect (e.g., U∂/∂x) and a non-Doppler effect [e.g., *Zhang and Webster*, 1989]. To simply our discussions, we only consider the Doppler effect, which gives the same dispersion relation, as the (ω) is replaced by (ω – kU). Figure A1a shows dispersion curves with different equivalent depths, from 8 m to 90 m, which are typical values in *Kiladis et al.* [2009]. These curves compare well with existing studies.

[56] From Figure A1b, which shows the periods in the k-H space, the corresponding periods with k = 12 but different H (from 20 to 90 m) are about 7∼8 days. Specifically, the period with k=12 and H=90m is about 7.08 days, which is consistent with Figure 5a. In Figure A1c, the dispersion relations with k = 12 but different H give phase speeds ranging from (−4.34) m/s to (−5.46) m/s. In Figure A1d, the "basic wind" is estimated by averaging the total zonal winds over a domain with a longitudinal width of 30° (which is the wavelength of the MRG wave) and over a period of 7 days (which is the period of the MRG wave). Two domains (red and blue boxes) with little differences in the number of latitudes are chosen, which give the averaged zonal wind speeds of 4.07 m/s and 3.28 m/s, respectively (Figure A1d). The domain-weighted averaged value of these two is 3.71 m/s. With the basic wind speeds of 3.71 m/s and the intrinsic phase speeds in Figure A1c, the Doppler-shifted phase speeds for k = 12 but different H range from −0.63 m/s to −1.75 m/s. Therefore, we obtained the close match of the westward phased speed (−1.8 m/s) to the linear shallow-water solution (−1.75 m/s) with k = 12 and H = 90 m. When the non-Doppler effect of a positive constant zonal mean flow is considered, it can increase the theoretical (westward) intrinsic phase speed, leading to a faster (westward) Doppler-shifted phase speed. Therefore, a theoretical phase speed with k=12 and H=90m may become larger than 1.8 m/s. However, consistency between the observed and theoretical phase speeds can be still maintained when a smaller value of H is selected. In addition to the non-Doppler effect, impact of both horizontal and vertical wind shears (e.g., the westerly wind burst associated with the MJO) should also be considered to obtain more realistic phase and group speeds that can be used as "ground truth." These are beyond the scope of this study.

[57] **Acknowledgments.** We would like to thank C. Schreck and two anonymous reviewers for their valuable suggestions, which have substantially improved the manuscript, and R. Anthes for his comments and encouragement. We are grateful for the support from the following organizations: the NASA Earth Science Technology Office (ESTO), the Advanced Information Systems Technology (AIST) Program, and the Modeling, Analysis and Prediction (MAP) Program. We would also like to thank Stephen Lang for proofreading this manuscript and K.-S. Kuo for preparing Figure 2. Acknowledgment is also made of the NASA High-End Computing (HEC) Program and of the NASA Advanced Supercomputing (NAS) division and NASA Center for Climate Simulation (NCCS) for the computer time used in this research.

References

Aiyyer, A. R., and J. Molinari (2003), Evolution of mixed Rossby-gravity waves in idealized MJO environments, *J. Atmos. Sci.*, *60*, 2837–2855, doi:10.1175/1520-0469(2003)060<2837:EOMRWI>2.0.CO;2.

Anthes, R. A. (2003), Hot towers and hurricanes: Early observations theories, and models, *Meteorol. Monogr.*, *51*, 139–148.

Atlas, R., O. Reale, B.-W. Shen, S.-J. Lin, J.-D. Chern, W. Putman, T. Lee, K.-S. Yeh, M. Bosilovich, and J. Radakovich (2005), Hurricane forecasting with the high-resolution NASA finite volume general circulation model, *Geophys. Res. Lett.*, *32*, L03807, doi:10.1029/2004GL021513.

Bengtsson, L., K. I. Hodges, and M. Esch (2007a), Tropical cyclones in a T159 resolution global climate model: Comparison with observations and re-analyses, *Tellus, Ser. A*, *59*(4), 396–416, doi:10.1111/j.1600-0870.2007.00236.x.

Bengtsson, L., K. I. Hodges, M. Esch, N. Keenlyside, L. Kornblueh, J.-J. Luo, and T. Yamagata (2007b), How may tropical cyclones change in a warmer climate?, *Tellus, Ser. A*, *59*(4), 539–561, doi:10.1111/j.1600-0870.2007.00251.x.

Bessafi, M., and M. C. Wheeler (2006), Modulation of South Indian Ocean tropical cyclones by the Madden-Julian oscillation and convectively coupled equatorial waves, *Mon. Weather Rev.*, *134*, 638–656, doi:10.1175/MWR3087.1.

Biswas, R., M. J. Aftosmis, C. Kiris, and B.-W. Shen (2007), Petascale computing: Impact on future NASA missions, in *Petascale Computing: Architectures and Algorithms*, edited by D. Bader, pp. 29–46, CRC, Boca Raton, Fla.

Braun, S. A., and W.-K. Tao (2001), Sensitivity of high-resolution simulations of Hurricane Bob (1991) to planetary boundary layer parameterizations, *Mon. Weather Rev.*, *128*, 3941–3961.

Chang, H.-R., and P. J. Webster (1995), Energy accumulation of emanation at low latitudes, Part III: Forward and backward accumulation, *J. Atmos. Sci.*, *52*, 2384–2403.

Charney, J. G., and A. Eliassen (1964), On the growth of the hurricane depression, *J. Atmos. Sci.*, *21*, 68–75, doi:10.1175/1520-0469(1964)021<0068:OTGOTH>2.0.CO;2.

Davis, C., and L. Bosart (2002), Numerical simulations of the genesis of Hurricane Diana (1984). Part II: Sensitivity of track and intensity prediction, *Mon. Weather Rev.*, *130*, 1100–1124, doi:10.1175/1520-0493(2002)130<1100:NSOTGO>2.0.CO;2.

Dickinson, M., and J. Molinari (2002), Mixed Rossby-gravity waves and western Pacific tropical cyclogenesis. Part I: Synoptic evolution, *J. Atmos. Sci.*, *59*, 2183–2196, doi:10.1175/1520-0469(2002)059<2183:MRGWAW>2.0.CO;2.

Dunkerton, T. J., M. T. Montgomery, and Z. Wang (2008), Tropical cyclogenesis in a tropical wave critical layer: Easterly waves, *Atmos. Chem. Phys. Discuss.*, *8*, 11,149–11,292, doi:10.5194/acpd-8-11149-2008.

Emanuel, K. A. (1986), An air-sea interaction theory for tropical cyclones. Part I, *J. Atmos. Sci.*, *43*, 585–605, doi:10.1175/1520-0469(1986)043<0585:AASITF>2.0.CO;2.

Ferreira, R. N., and W. H. Schubert (1996), Dynamical aspects of twin tropical cyclones associated with the Madden-Julian oscillation, *J. Atmos. Sci.*, *53*, 929–945, doi:10.1175/1520-0469(1996)053<0929:DAOTTC>2.0.CO;2.

Frank, W. M., and P. E. Roundy (2006), The role of tropical waves in tropical cyclogenesis, *Mon. Weather Rev.*, *134*, 2397–2417, doi:10.1175/MWR3204.1.

Gall, J. S., W. M. Frank, and M. C. Wheeler (2010), The role of equatorial Rossby waves in tropical cyclogenesis. Part I: Idealized numerical simulations in an initially quiescent background environment, *Mon. Weather Rev.*, *138*, 1368–1382, doi:10.1175/2009MWR3114.1.

Hack, J. J. (1994), Parameterization of moist convection in the NCAR CCM2, *J. Geophys. Res.*, *99*, 5551–5568, doi:10.1029/93JD03478.

Hendricks, E. A., M. T. Montgomery, and C. A. Davis (2004), The role of "vortical" hot towers in the formation of tropical cyclone Diana (1984), *J. Atmos. Sci.*, *61*, 1209–1232, doi:10.1175/1520-0469(2004)061<1209:TROVHT>2.0.CO;2.

Holland, G., and P. Webster (2005), Scale interaction and tropical cyclone genesis; why global models have skill, paper presented at 59th Interdepartmental Hurricane Conference, Univ. of N. Fla., Jacksonville.

Holton, J. (1975), On the influence of boundary layer friction on mixed Rossby-gravity waves, *Tellus*, *27*, 107–115, doi:10.1111/j.2153-3490.1975.tb01664.x.

Huffman, G. J., R. F. Adler, D. T. Bolvin, G. Gu, E. J. Nelkin, K. P. Bowman, Y. Hong, E. F. Stocker, and D. B. Wolff (2007), The TRMM multisatellite precipitation analysis (TMPA): Quasi-global, multiyear, combined-sensor precipitation estimates at fine scales, *J. Hydrometeorol.*, *8*, 38–55, doi:10.1175/JHM560.1.

Keen, R. A. (1982), The role of cross-equatorial tropical cyclone pairs in the Southern Oscillations, *Mon. Weather Rev.*, *110*, 1405–1416, doi:10.1175/1520-0493(1982)110<1405:TROCET>2.0.CO;2.

Kerr, R. (2006), Sharpening up models for a better view of the atmosphere, *Science*, *313*, 1040, doi:10.1126/science.313.5790.1040.

Kiladis, G. N., M. C. Wheeler, P. T. Haertel, K. H. Straub, and P. E. Roundy (2009), Convectively coupled equatorial waves, *Rev. Geophys.*, *47*, RG2003, doi:10.1029/2008RG000266.

Lander, M. (1990), Evolution of the cloud pattern during the formation of tropical cyclone twins symmetrical with respect to the equator, *Mon. Weather Rev.*, *118*, 1194–1202, doi:10.1175/1520-0493(1990)118<1194:EOTCPD>2.0.CO;2.

Liebmann, B., and H. H. Hendon (1990), Synoptic-scale disturbances near the equator, *J. Atmos. Sci.*, *47*, 1463–1479, doi:10.1175/1520-0469(1990)047<1463:SSDNTE>2.0.CO;2.

Liebmann, B., H. H. Hendon, and J. D. Glick (1994), The relationship between tropical cyclones of the western Pacific and Indian oceans and the Madden-Julian Oscillation, *J. Meteorol. Soc. Jpn.*, *72*, 401–412.

Lin, S.-J. (2004), A vertically Lagrangian finite-volume dynamical core for global models, *Mon. Weather Rev.*, *132*, 2293–2307, doi:10.1175/1520-0493(2004)132<2293:AVLFDC>2.0.CO;2.

Lin, S.-J., B.-W. Shen, W. P. Putman, and J.-D. Chern (2003), Application of the high-resolution finite-volume NASA/NCAR Climate Model for Medium-Range Weather Prediction Experiments, paper presented at EGS-AGU-EUG Joint Assembly, EGS, Nice, France.

Lin, Y.-L. (2007), *Mesoscale Dynamics*, 630 pp., Cambridge Univ. Press, Cambridge, U. K., doi:10.1017/CBO9780511619649.

Lindzen, R. S., and T. Matsuno (1968), On the nature of large-scale wave disturbances in the equatorial lower stratosphere, *J. Meteorol. Soc. Jpn.*, *46*, 215–221.

Liu, W. T., W. Tang, and P. S. Polito (1998), NASA Scatterometer provides global ocean-surface wind fields with more structures than numerical weather prediction, *Geophys. Res. Lett.*, *25*, 761–764, doi:10.1029/98GL00544.

Madden, R. A., and P. R. Julian (1994), Observations of the 40–50-day tropical oscillation—A review, *Mon. Weather Rev.*, *122*, 814–837, doi:10.1175/1520-0493(1994)122<0814:OOTDTO>2.0.CO;2.

Maloney, E. D., and D. L. Hartmann (2000), Modulation of eastern North Pacific hurricanes by the Madden-Julian oscillation, *J. Clim.*, *13*, 1451–1460, doi:10.1175/1520-0442(2000)013<1451:MOENPH>2.0.CO;2.

Maruyama, T. (1967), Large scale disturbances in the equatorial lower stratosphere, *J. Meteorol. Soc. Jpn.*, *45*, 391–408.

Matsuno, T. (1966), Quasi-geostrophic motions in the equatorial area, *J. Meteorol. Soc. Jpn.*, *44*, 25–43.

Molinari, J., and M. Dudek (1992), Parameterization of convective precipitation in mesoscale numerical models: A critical review, *Mon. Weather Rev.*, *120*, 326–344, doi:10.1175/1520-0493(1992)120<0326:POCPIM>2.0.CO;2.

Molinari, J., K. Lombardo, and D. Vollaro (2007), Tropical cyclogenesis within an equatorial Rossby wave packet, *J. Atmos. Sci.*, *64*, 1301–1317, doi:10.1175/JAS3902.1.

Moncrieff, M. W., M. A. Shapiro, J. M. Slingo, and F. Molteni (2007), Organized tropical convection and the global circulation: Collaborative research at the intersection of weather and climate, *WMO Bull.*, *56*(3), 1–9.

Montgomery, M. T., M. E. Nicholls, T. A. Cram, and A. Saunders (2006), A "vortical" hot tower route to tropical cyclogenesis, *J. Atmos. Sci.*, *63*, 355–386, doi:10.1175/JAS3604.1.

Nolan, D. (2007), What is the trigger for tropical cyclogenesis?, *Aust. Meteorol. Mag.*, *56*, 241–266.

Ooyama, K. (1964), A dynamical model for the study of tropical cyclone development, *Geofis. Int.*, *4*, 187–198.

Ooyama, K. (1969), Numerical simulation of the life cycle of tropical cyclones, *J. Atmos. Sci.*, *26*, 3–40, doi:10.1175/1520-0469(1969)026<0003:NSOTLC>2.0.CO;2.

Ooyama, K. (1982), Conceptual Evolution of the theory and modeling of the tropical cyclone, *J. Meteorol. Soc. Jpn.*, *60*, 369–379.

Pan, H.-L., and W.-S. Wu (1995), Implementing a mass flux convection parameterization package for the NMC medium-range forecast model, *NMC Off. Note 409*, 40 pp., NCEP, Camp Springs, Md.

Schreck, C. J., and J. Molinari (2009), A case study of an outbreak of twin tropical cyclones, *Mon. Weather Rev.*, *137*, 863–875, doi:10.1175/2008MWR2541.1.

Schreck, C. J., J. Molinari, and A. Aiyyer (2012), A global view of equatorial waves and tropical cyclogenesis, *Mon. Weather Rev.*, *140*, 774–788, doi:10.1175/MWR-D-11-00110.1.

Shen, B.-W., R. Atlas, J.-D. Chern, O. Reale, S.-J. Lin, T. Lee, and J. Change (2006a), The 0.125 degree finite volume general mesoscale circulation model: Preliminary simulations of mesoscale vortices, *Geophys. Res. Lett.*, *33*, L05801, doi:10.1029/2005GL024594.

Shen, B.-W., R. Atlas, O. Reale, S.-J. Lin, J.-D. Chern, J. Chang, C. Henze, and J.-L. Li (2006b), Hurricane forecasts with a global mesoscale-resolving model: Preliminary results with Hurricane Katrina (2005), *Geophys. Res. Lett.*, *33*, L13813, doi:10.1029/2006GL026143.

Shen, B.-W., et al. (2006c), Hurricane forecasts with a global mesoscale model on the NASA Columbia supercomputer, *Eos Trans. AGU*, *87*(52), Fall Meet. Suppl., Abstract A13E-0986.

Shen, B.-W., W.-K. Tao, W. K. Lau, and R. Atlas (2010a), Predicting tropical cyclogenesis with a global mesoscale model: Hierarchical multiscale interactions during the formation of tropical cyclone Nargis (2008), *J. Geophys. Res.*, *115*, D14102, doi:10.1029/2009JD013140.

Shen, B.-W., W.-K. Tao, and M.-L. C. Wu (2010b), African easterly waves in 30-day high-resolution global simulations: A case study during the 2006 NAMMA period, *Geophys. Res. Lett.*, *37*, L18803, doi:10.1029/2010GL044355.

Smagorinsky, J. (1967), The role of numerical modeling, *Bull. Am. Meteorol. Soc.*, *46*, 89–93.

Straub, K. H., and G. N. Kiladis (2003), Interactions between the boreal summer intraseasonal oscillation and higher-frequency tropical wave activity, *Mon. Weather Rev.*, *131*, 945–960, doi:10.1175/1520-0493(2003)131<0945:IBTBSI>2.0.CO;2.

Sundqvist, H. (1988), Parameterization of condensation and associated clouds in models for weather prediction and general circulation simulation, in *Physically-Based Modeling and Simulation of Climate and Climatic Change*, vol. 1, edited by M. E. Schlesinger, pp. 433–461, Kluwer Acad., Norwell, Mass.

Takayabu, Y. N., and T. Nitta (1993), 3–5 day-period disturbances coupled with convection over the tropical Pacific Ocean, *J. Meteorol. Soc. Jpn.*, *71*, 221–246.

Tory, K. J., M. T. Montgomery, and N. E. Davidson (2006a), Prediction and diagnosis of tropical cyclone formation in an NWP system. Part I: The critical role of vortex enhancement in deep convection, *J. Atmos. Sci.*, *63*, 3077–3090, doi:10.1175/JAS3764.1.

Tory, K. J., et al. (2006b), Prediction and diagnosis of tropical cyclone formation in an NWP system. Part II: A diagnosis of tropical cyclone Chris formation, *J. Atmos. Sci.*, *63*, 3091–3113, doi:10.1175/JAS3765.1.

Vitart, E., et al. (2001), Sensitivity of tropical storms simulated by a general circulation model to changes in cumulus parameterization, *Q. J. R. Meteorol. Soc.*, *127*, 25–51, doi:10.1002/qj.49712757103.

Webster, P. J., and H.-R. Chang (1988), Equatorial energy accumulation and emanation regions: Impacts of a zonally varying basic state, *J. Atmos. Sci.*, *45*, 803–829, doi:10.1175/1520-0469(1988)045<0803:EEAAER>2.0.CO;2.

Wheeler, M., G. N. Kiladis, and P. J. Webster (2000), Large-scale dynamical fields associated with convectively coupled equatorial waves, *J. Atmos. Sci.*, *57*, 613–640, doi:10.1175/1520-0469(2000)057<0613:LSDFAW>2.0.CO;2.

World Meteorological Organization (WMO) (2004), WMO/ESCAP Panel on Tropical Cyclones annual review 2002, report, 76 pp., Geneva, Switzerland. [Available at http://www.preventionweb.net/files/1527_7895.pdf.]

Zhang, C., and P. J. Webster (1989), Effects of zonal flows on equatorially trapped waves, *J. Atmos. Sci.*, *46*, 3632–3652, doi:10.1175/1520-0469(1989)046<3632:EOZFOE>2.0.CO;2.

Zhang, G. J., and N. A. McFarlane (1995), Sensitivity of climate simulations to the parameterization of cumulus convection in the Canadian Climate Center general circulation model, *Atmos. Ocean*, *33*, 407–446, doi:10.1080/07055900.1995.9649539.

Zhang, Q., J. Gottschalck, and Y. Xue (2007), Extension of The CPC MJO Index to forecast mode, paper presented at 16th Conference on Applied Climatology, Am. Meteorol. Soc., San Antonio, Tex. [Available at http://ams.confex.com/ams/pdfpapers/117716.pdf.]

Correction to "Genesis of twin tropical cyclones as revealed by a global mesoscale model: The role of mixed Rossby gravity waves"

Bo-Wen Shen, Wei-Kuo Tao, Yuh-Lang Lin, and Arlene Laing

In the paper "Genesis of twin tropical cyclones as revealed by a global mesoscale model: The role of mixed Rossby gravity waves" by Bo-Wen Shen et al. (*Journal of Geophysical Research, 117*, D13114, doi:10.1029/2011JD017450, 2012), errors were introduced to Figures 4, 6, 10, and 21 during production. The correct figures and captions are given below.

Figure 4. Initial conditions in terms of wind vectors and geopotential heights at (a) 850-hpa and (b) 500-hpa from the NCEP T254 analyses. (c) The same as Figure 4a except for the NCEP 2.5° reanalysis. (d) The difference in 850-hpa winds (vectors) and geopotential heights (with contour lines of 6 and 8) between the NCEP T254 analyses and 2.5° reanalysis. This shows the dependence of the resolved MRG wave.

Figure 6. The 850-hPa winds (vectors) and geo-potential heights (shaded) at 0000 UTC 3–5 May 2002 from (a, c, and e) NCEP T254 analyses and (b, d, and f) the control run. There were three gyres with cyclonic circulation centers, S1 N1 and S2. A reduction in the MRG wavelength can be seen by the reduced distance between gyres S1 and S2. During the period of MRG wave intensification, the northern vortex moved poleward in association with a northward extension of the MRG wave and later developed into TC 01A. The gray oval in Figure 6c indicates the circulation of gyre S2 which is similar to that of a MRG wave in Figure 3c.

Figure 10. Longitude-height cross sessions of meridional winds at 0000 UTC 4 May 2002 averaged over latitudes (a and c) 5°S to the equator and (b and d) from the equator to 5°N. Figures 10a and 10b show the NCEP T254 analyses while Figures 10c and 10d show the control run. S2 and N1 roughly indicated the location of the gyres.

Figure 21. Hovmoller diagram of the vorticity ($10^{-5}s^{-1}$). Shaded areas show vorticities averaged over latitudes 10°S and 0°, while contour lines (with selected values of 1, 2, 4, and $6 \times 10^{-5}s^{-1}$) show vorticities averaged over latitudes 0° and 10°N. (a) The CNTL run, (b) the EXP-A run, (c) the EXP-B run, and (d) the EXP-C run. Local minima (blue) indicate the locations of gyre S1 and gyre S2. Dense contour lines between gyres S1 and S2 indicate the location of gyre N1.

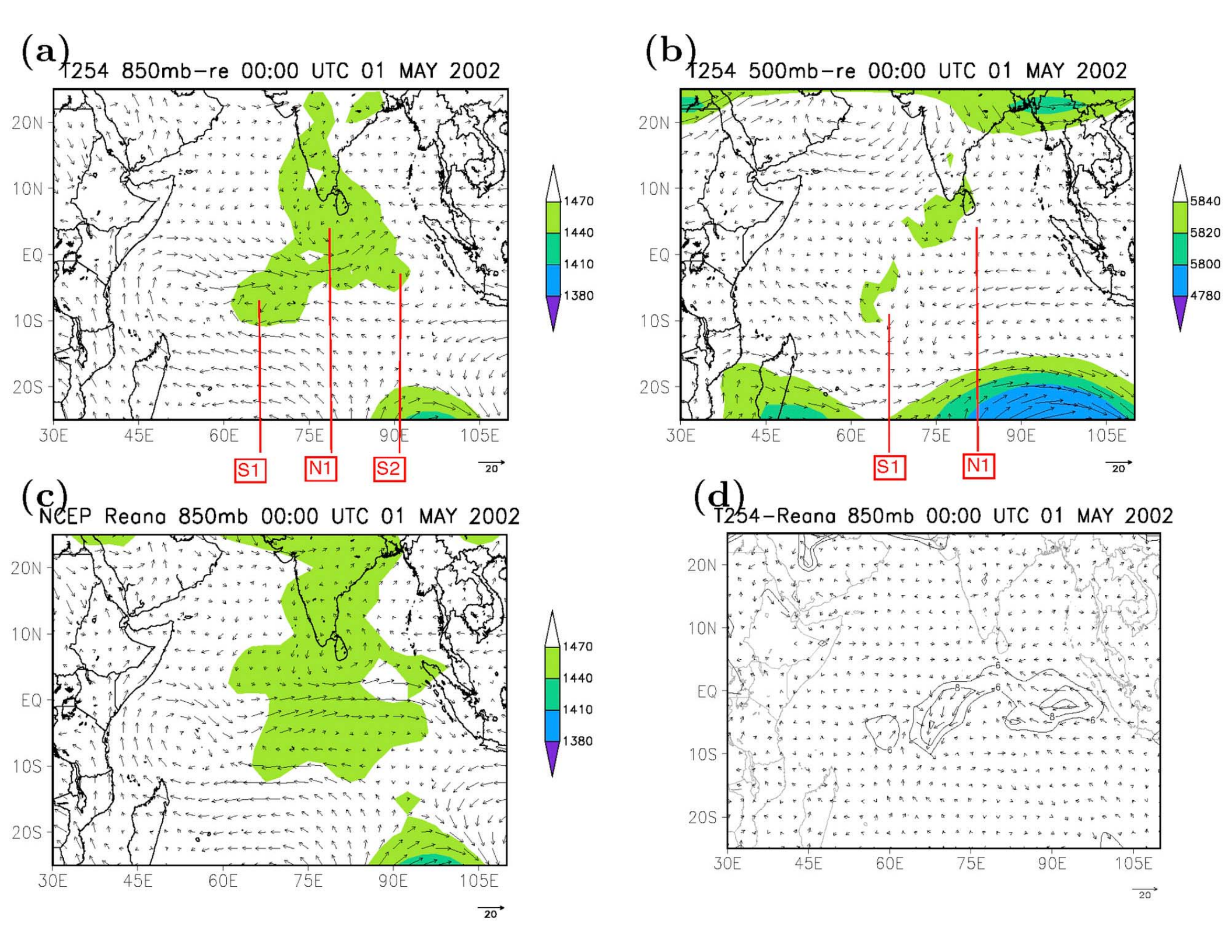
(a)
T254 850mb-re 00:00 UTC 01 MAY 2002
20N
10N
EQ
10S
20S
30E
45E
60E
75E
90E
105E
S1
N1
S2
1470
1440
1410
1380
20
(b)
T254 500mb-re 00:00 UTC 01 MAY 2002
20N
10N
EQ
10S
20S
30E
45E
60E
75E
90E
105E
S1
N1
5840
5820
5800
4780
20
(c)
NCEP Reana 850mb 00:00 UTC 01 MAY 2002
20N
10N
EQ
10S
20S
30E
45E
60E
75E
90E
105E
1470
1440
1410
1380
20
(d)
T254-Reana 850mb 00:00 UTC 01 MAY 2002
20N
10N
EQ
10S
20S
30E
45E
60E
75E
90E
105E
6
8
20

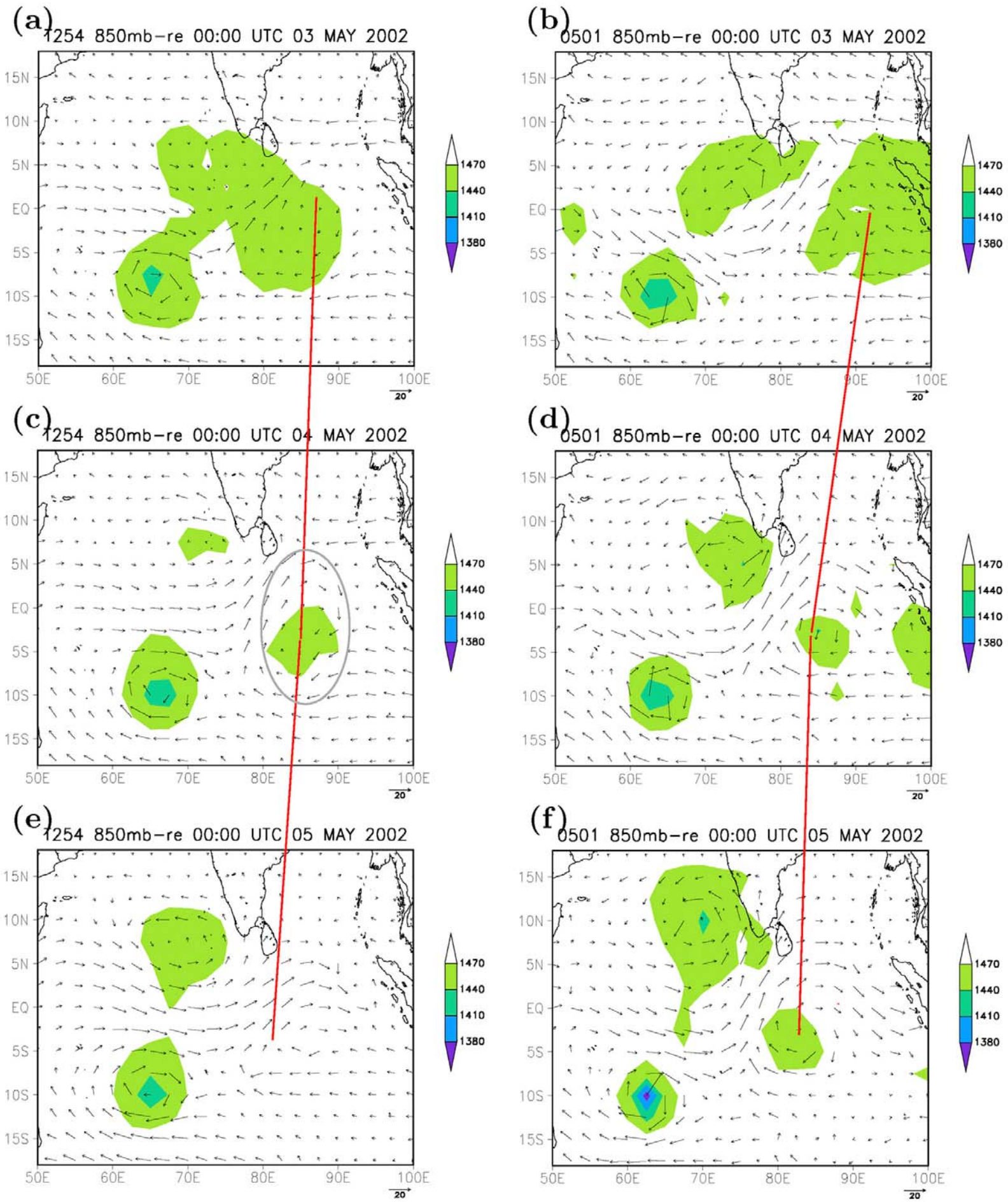
(a)
1254 850mb−re 00:00 UTC 03 MAY 2002
(b)
0501 850mb−re 00:00 UTC 03 MAY 2002
(c)
1254 850mb−re 00:00 UTC 04 MAY 2002
(d)
0501 850mb−re 00:00 UTC 04 MAY 2002
(e)
1254 850mb−re 00:00 UTC 05 MAY 2002
(f)
0501 850mb−re 00:00 UTC 05 MAY 2002
15N
10N
5N
EQ
5S
10S
15S
50E
60E
70E
80E
90E
100E
20
1470
1440
1410
1380

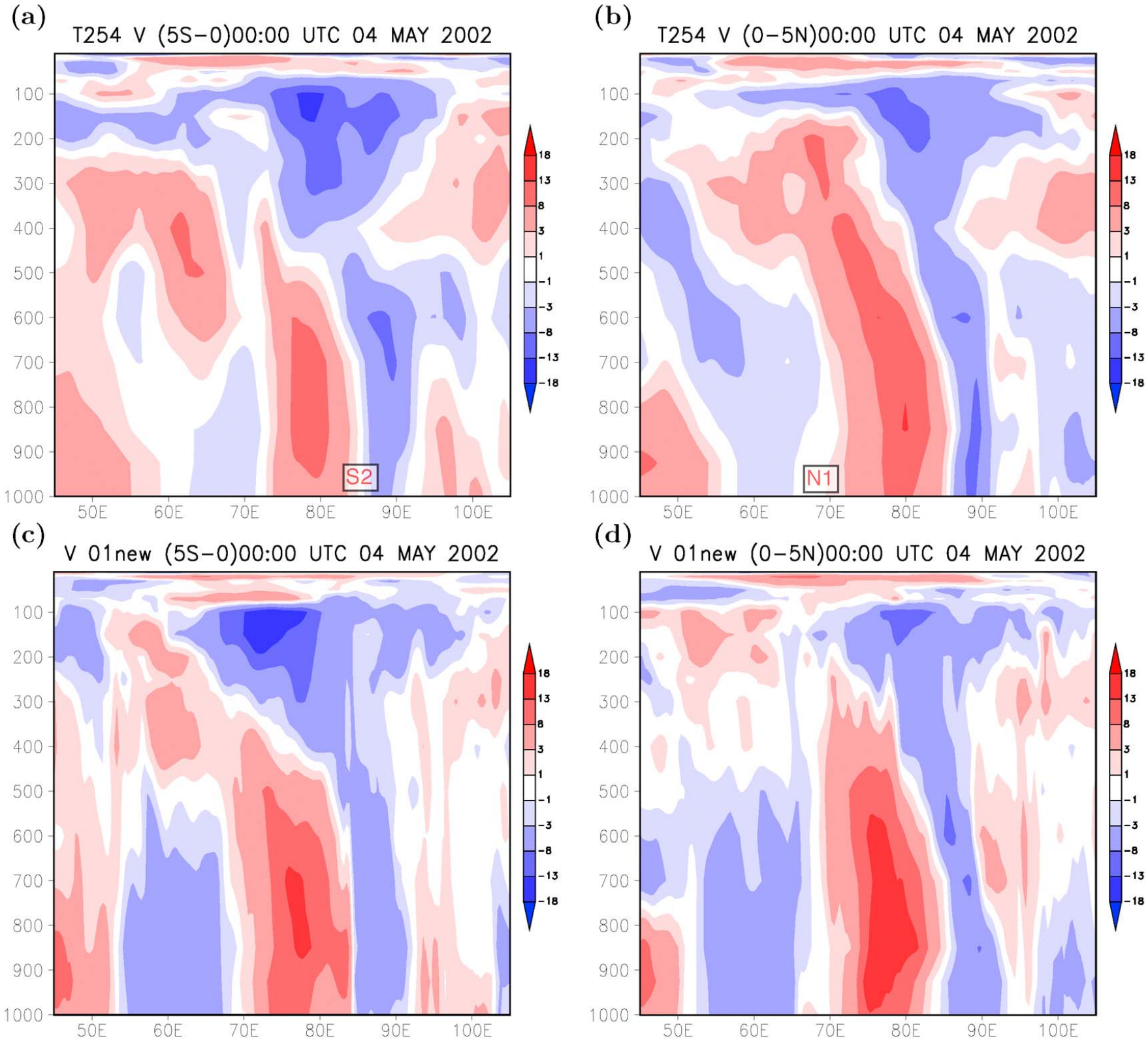
(a)
T254 V (5S-0)00:00 UTC 04 MAY 2002
S2
(b)
T254 V (0-5N)00:00 UTC 04 MAY 2002
N1
(c)
V 01new (5S-0)00:00 UTC 04 MAY 2002
(d)
V 01new (0-5N)00:00 UTC 04 MAY 2002
100
200
300
400
500
600
700
800
900
1000
50E
60E
70E
80E
90E
100E
18
13
8
3
1
-1
-3
-8
-13
-18

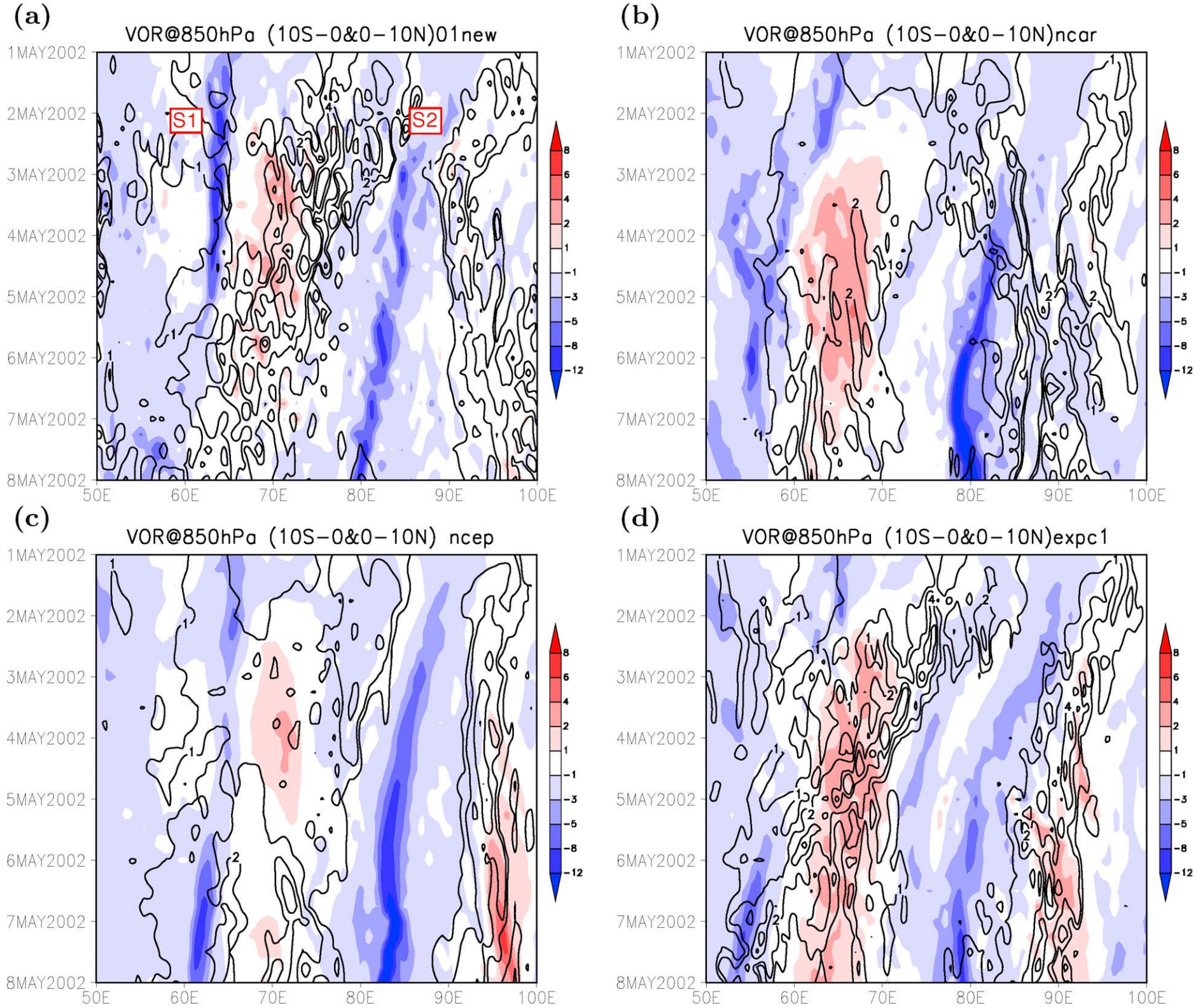
(a)
VOR@850hPa (10S-0&0-10N)01new
S1
S2
(b)
VOR@850hPa (10S-0&0-10N)ncar
(c)
VOR@850hPa (10S-0&0-10N) ncep
(d)
VOR@850hPa (10S-0&0-10N)expc1
1MAY2002
2MAY2002
3MAY2002
4MAY2002
5MAY2002
6MAY2002
7MAY2002
8MAY2002
50E
60E
70E
80E
90E
100E
8
6
4
2
1
-1
-3
-5
-8
-12

Thank you for evaluating Wondershare PDF Merger! To remove this page, please register your program!

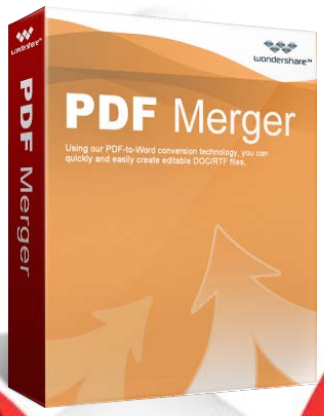

Go to Purchase Now>>

PDF Merger

- ✓ Merge multiple PDF files into one
- ✓ Select page range of PDF to merge
- ✓ Select specific page(s) to merge
- ✓ Extract page(s) from different PDF files and merge into one